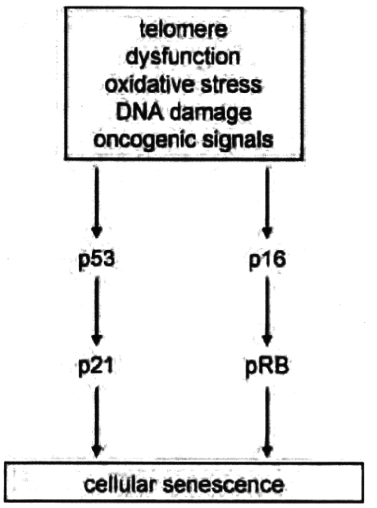

Figure 2. Regulation of cellular senescence by p53- and pRB-dependent pathways. Replicate senescence induced by telomere dysfunction and stress-induced cellular senescence induced by various stresses or oncogenic signals are mediated by p53- and pRB-dependent pathways. p21 is a direct target of p53 and mediates p53-induced cell cycle arrest. p16 inhibits pRB phosphorylation, which results in the inhibition of E2F-dependent gene transcription necessary for cell cycle progression.

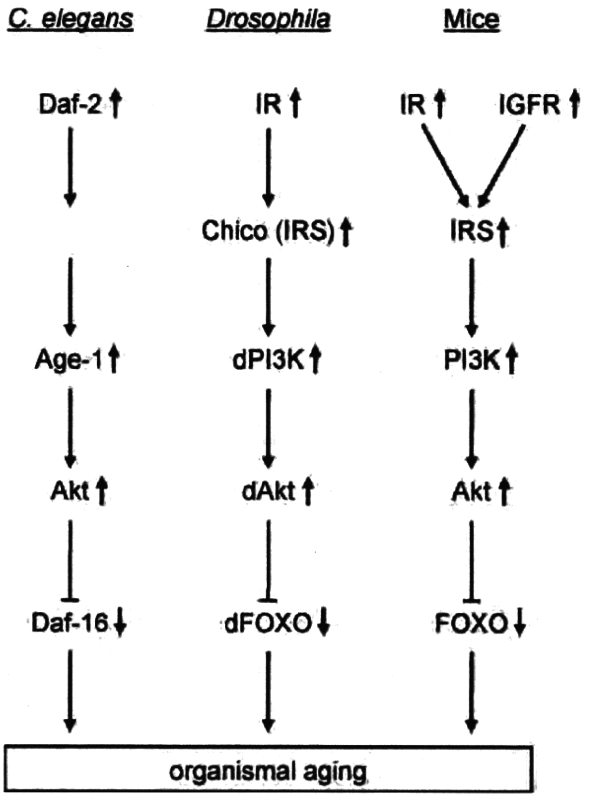

Figure 3. Regulation of organismal aging by insulin/IGF-PI3K-Akt-FOXO pathway in multiple species. The finding that *daf-2* mutations extend lifespan of the nematode *C elegans* led to the identification of insulin/IGF signaling as a critical regulatory pathway that controls organismal aging in multiple species. All mutations that extend lifespan downregulates this signaling axis, leading to increased activity of FOXO/Daf-16. Insulin/IGF signaling therefore promotes organismal aging through down-regulation of FOXO/Daf-16.

dependent kinase-mediated pRB phosphorylation. In senescent cells, p16 is upregulated, pRB is hypophosphorylated, and E2F target genes are repressed.[14,16,17] Although inactivation of p16 does not prevent replicative senescence, p16 is required for senescence induced by RAS and other stresses.[8,16] Thus, it is conceivable that p53-p21 pathway primarily regulates cellular senescence attributable to telomere dysfunction, whereas p16-pRB pathway preferentially regulates stress-induced premature senescence. p16 is upregulated during organismal aging, and the number of p16-positive cells increases with age. Together with senescence-associated β-galactosidase activity,[18] p16 is a well-established biomarker of senescent cells.[8,19] In addition to these classic markers of cellular senescence, Binet et al recently reported that Wnt16B is a marker of senescent cells.[20] Wnt16B is overexpressed in cells undergoing replicative or stress-induced senescence in vitro and those in K-Ras–induced adenomas in vivo, and forced expression of Wnt16B accelerates, whereas knockdown of Wnt16B attenuates, the onset of cellular senescence. However, because these authors failed to detect the activation of Wnt/β-catenin signaling by Wnt16B, the link between Wnt signaling and cellular senescence is not evident in this context.

One intriguing question is whether cellular senescence plays a causal role in organismal aging. As mentioned above, the number of senescent cells detected by p16 expression and/or senescence-associated β-galactosidase activity is increased with age in multiple tissues in humans and rodents.[8,16,17] Moreover, these cells are observed at sites of various age-related pathologies.[21–25] Thus, although these observations are correlative and do not directly demonstrate that organismal aging is attributable to an increase in senescent cells, cellular senescence may, in part, contribute to the pathogenesis of aging-related phenotypes or diseases.

Organismal Aging

Organismal aging is usually defined as the progressive decline in the function of multiple organs to maintain baseline tissue homeostasis and to adequately respond to environmental stresses.[26] Genetic dissection of aging was greatly advanced by the identification of mutations that extend lifespan of the nematode *Caenorhabditis elegans*,[27] and it is now evident that aging process in various organisms is regulated by evolutionarily conserved signaling pathways.[28] The most extensively investigated signaling pathway that regulates lifespan is the insulin/insulin-like growth factor (IGF) pathway.[29,30] In *C elegans*, mutations in *daf-2* was shown to double the lifespan and a *daf-16* gene product was required for the lifespan extension by *daf-2* mutations.[27] *daf-2* encodes an insulin/IGF receptor ortholog,[31] and *daf-16* encodes a FOXO family of forkhead transcription factor.[32,33] Moreover, mutations of *age-1*, which encodes phosphatidylinositol-3 kinase (PI3K) catalytic subunit, also extend the lifespan of *C elegans*,[34] and *C elegans* Akt was shown to antagonize the activity of DAF-16.[35] In *Drosophila*, mutations in the gene

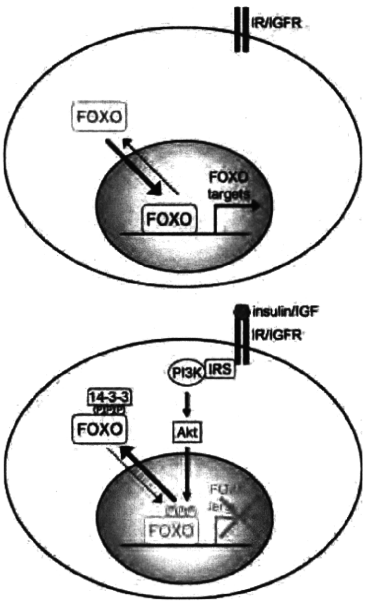

Figure 4. Regulation of FOXO/Daf-16 transcriptional activity by insulin/IGF signaling. FOXO/Daf-16 is constantly shuttling between the cytoplasm and the nucleus. When insulin/IGF signaling is downregulated, FOXO/Daf-16 translocates to the nucleus and activates its target genes **(top)**. However, when insulin/IGF signaling is activated, FOXO/Daf-16 is phosphorylated by Akt, which creates a binding site for 14-3-3 proteins and results in nuclear exclusion of FOXO/Daf-16 **(bottom)**.

encoding an insulin/IGF receptor or those of *chico* gene encoding an insulin receptor substrate (IRS)-like protein result in lifespan extension.[36–38] In mice, heterozygous deletion of *igf1r* gene encoding type1 IGF receptor, adipose tissue-specific deletion of insulin receptor gene, and brain-specific deletion of *irs2* gene all result in extension of lifespan.[39–41] These results collectively suggest that the conserved insulin/IGF-IRS-PI3K-Akt-FOXO signaling axis regulates lifespan in multiple organisms (Figure 3).

Because insulin/IGF signaling downregulates FOXO/DAF-16 through Akt-mediated phosphorylation (Figure 4), mutations that extend lifespan lead to upregulation of FOXO/DAF-16 activity, suggesting that FOXO/DAF-16 targets are downstream effectors that influence lifespan. Candidate FOXO/DAF-16 targets include genes involved in oxidative stress response (superoxide dismutase, catalase), cell cycle arrest (p27), and DNA repair (Gadd45).[42–45] Of note, overexpression of superoxide dismutase or catalase induces the extension of lifespan in *Drosophila*,[46] and overexpression of catalase targeted to mitochondria results in lifespan extension in mice.[47] Although the target genes of FOXO/DAF-16 that are thought to affect lifespan are increasing in number,[48,49] it is conceivable that one mechanism of lifespan extension by mutations in insulin/IGF pathway is the increased stress resistance conferred by FOXO/DAF-16.

Wnt Signaling and Aging

In 2007, 3 studies directly linked β-catenin–dependent canonical Wnt signaling to cellular senescence or organismal aging.[50–52] Ye et al provided evidence showing that cellular senescence of human diploid fibroblast cell line WI-38 was triggered by downregulation of *Wnt2* gene.[50] The authors found that *Wnt2* gene expression was downregulated in senescent cells and, as a consequence, GSK-3β kinase activity was upregulated and cytosolic β-catenin levels were downregulated in senescent cells. The authors also showed that inhibition of Wnt signaling induced premature senescence, whereas activation of Wnt signaling promoted cell proliferation and delayed replicative or RAS-induced senescence. Mechanistically, downregulation of *Wnt2* leads to increased kinase activity of GSK-3β, which results in increased phosphorylation and enhanced recruitment of HIRA to acute promyelocytic leukemia nuclear bodies. HIRA is a histone chaperone, and translocation of this protein to promyelocytic leukemia nuclear bodies is the initial step for the formation of SAHF (senescent-associated heterochromatin foci), which is a distinct heterochromatin structure specifically observed in senescent cells.[53,54] Taken together, these observations suggest that canonical Wnt signaling inhibits cellular senescence through inactivation of GSK-3β. It remains to be elucidated how Wnt signaling is downregulated in the initial phase of cellular senescence. Furthermore, given the conserved role of insulin/IGF signaling in organismal aging, it will be interesting to test whether HIRA phosphorylation and SAHF formation are increased by insulin/IGF that inactivates GSK-3β through Akt-dependent phosphorylation.

In contrast to Ye et al,[50] 2 studies demonstrated that canonical Wnt signaling rather promotes mammalian aging and aging-related phenotypes.[51,52] Liu et al[51] used the *klotho* mouse model of accelerated aging, in which *klotho* gene expression is severely impaired.[55] *Klotho* gene encodes a type I transmembrane protein with a large extracellular domain that is cleaved by ADAM family of proteases.[56] The resultant secreted form of Klotho protein was shown to directly bind to Wnt3 and inhibit canonical Wnt signaling. The activity of Wnt signaling was increased in *klotho* mice, which was associated with decreased number of stem cell population and increased number of senescent cells in the skin and the small intestine. Moreover, continuous exposure to Wnt3A induced cellular senescence in mouse embryonic fibroblasts, and overexpression of Wnt1 in the skin resulted in increased expression of senescence markers in hair follicle stem cells. These findings suggest that activation of canonical Wnt signaling plays a causal role in premature aging in *klotho* mice. It should be noted, however, that Klotho protein was shown to inhibit insulin/IGF signaling and mediate FGF23 signaling as a coreceptor for FGF23, and both of these signaling pathways are implicated in the regulation of lifespan and aging-related pathology.[56,57] Thus, the extent to which the increased Wnt activity contributes to premature aging phenotypes in *klotho* mice is unclear.

A decline in tissue regenerative capacity is a hallmark of mammalian aging and is, in part, attributed to the impairment of tissue stem/progenitor cell function. It was previously shown that the age-related decline in tissue-specific progenitor cell activity is modulated by factors that are present in the serum.[58] In line with this study, Brack et al[52] provided evidence showing that systemic factors in the serum of aged mice activate canonical Wnt signaling and contribute to

age-related decline in skeletal muscle regeneration. The authors showed that skeletal muscle stem cells (satellite cells) convert from a myogenic to a fibrogenic lineage when exposed to aged serum and that canonical Wnt signaling is enhanced in skeletal muscle of aged mice and in cultured satellite cells exposed to aged serum. Moreover, skeletal muscle regeneration in young animals was attenuated by Wnt3A treatment, whereas impaired muscle regeneration in aged mice was restored by inhibition of canonical Wnt signaling. These observations suggest that activation of Wnt signaling by the "Wnt-like substance" present in the serum of aged organisms contributes to a decline in tissue stem cell function and impaired tissue regeneration associated with aging. The nature of this Wnt-like substance in the serum is unknown at present and remains to be elucidated. Because Wnt proteins are tightly associated with the cell surface and/or extracellular matrix and are thought to act in a short-range manner,[3,59] it is presumed that the Wnt-like substance in the serum are distinct from conventional Wnt proteins.

How can we reconcile the apparent discrepancies among these three studies? The conclusion of the study by Ye et al[50] depends solely on the results of cell culture experiments, whereas the conclusions by Liu et al[51] and Brack et al[52] deal with premature aging or aging-associated phenotypes in mice. This difference in the experimental system may be one explanation for the discrepancy. In addition, it was previously shown that Wnt signaling has pleiotropic and sometimes antagonistic effects on multiple biological processes, depending on the timing, strength, and duration of the signal. For instance, Wnt signaling promotes self-renewal and expansion of hematopoietic stem cells,[60,61] whereas constitutive activation of this signaling pathway in hematopoietic stem cells resulted in a rapid exhaustion of long-term stem cell pool and widespread hematologic abnormalities.[62,63] Likewise, it was shown in one study that β-catenin functions as a cofactor for FOXO/DAF-16 and promotes FOXO/DAF-16-dependent resistance against oxidative stress,[64] whereas another study demonstrated that Wnt signaling activates mitochondrial biogenesis and promotes the production of reactive oxygen species.[65] It was also shown in young animals that Wnt activation is required for myogenic specification of $CD45^+$ resident stem cells during muscle regeneration and that Wnt signaling promotes de novo hair follicle regeneration after skin wounding,[66,67] suggesting that downstream targets of Wnt signaling may change with age. Taken together, another explanation for the discrepancy among the 3 studies mentioned above may be the cell-, tissue-, and stage-specific pleiotropic effects of Wnt signaling on cellular senescence, organismal aging, and tissue regeneration (Figure 5).

Wnt Signaling and Age-Related Heart Disorders

The incidence of left ventricular hypertrophy, diastolic dysfunction, and atrial fibrillation increase with age.[6] Aging is also associated with an increase in intimal thickening and vessel stiffness that precede clinical diseases.[68] The observation that some systemic factors activate Wnt pathway in aged animals suggests that cells in the aged heart are also targets of

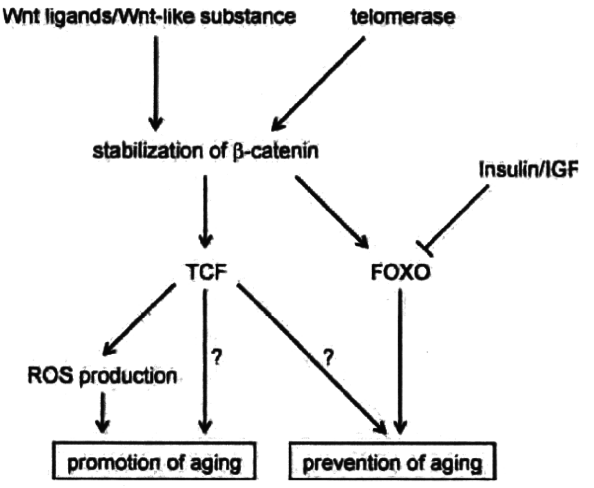

Figure 5. Possible involvement of Wnt signaling in organismal aging. β-Catenin–dependent canonical Wnt signaling is activated by conventional Wnt ligands, Wnt-like substance in the serum, and in some situations by telomerase, leading to β-catenin stabilization and nuclear translocation. Activation of canonical Wnt signaling may prevent aging by activating FOXO-dependent transcription or through unidentified TCF targets. Canonical Wnt signaling may also promote aging by enhancing mitochondrial biogenesis and reactive oxygen species (ROS) production or through other unidentified TCF targets.

Wnt signaling.[51] Indeed, aged TOPGAL mice (a transgenic mice in which β-galactosidase transgene is under the control of multimerized TCF binding sites) exhibit increased β-galactosidase expression in the heart, indicative of increased activity of Wnt signaling in the aged heart (our unpublished observation, 2009).

Wnt Activation in Myocytes

Cardiomyocyte hypertrophy is one of the characteristic features of aged heart. It was previously shown that stabilization of β-catenin promotes myocyte growth and is required for both physiological and pathological cardiac hypertrophy.[69,70] Subsequently, activation of Wnt signaling in cardiac myocytes in vivo was achieved by cardiomyocyte-specific conditional deletion of exon 3 of the β-catenin gene, which renders β-catenin resistant to GSK-3β–mediated phosphorylation/degradation and results in β-catenin stabilization.[71] These mice exhibit impaired cardiac growth with normal contractile function at baseline and attenuated hypertrophic growth response and impaired contractility following continuous angiotensin II infusion.[71] Thus, contrary to the previous studies, it was suggested that Wnt activation in cardiac myocytes results in attenuated response to hypertrophic stimuli and failure to undergo adaptive remodeling under stressed conditions. The precise reason for such discrepancy is unknown but may reflect the pleiotropic effects of Wnt signaling depending on the experimental conditions. It should also be noted that downregulation of Wnt/β-catenin signaling in cardiac myocytes is implicated in fibrofatty replacement of the myocardium observed in arrhythmogenic right ventricular cardiomyopathy.[72,73] Whether Wnt activation in cardiac myocytes contributes to aging-associated disorders in the heart remains to be elucidated.

Wnt Activation in Fibroblasts

Cardiac fibrosis is another feature of the aged heart[74] and is linked to the pathogenesis of atrial fibrillation and diastolic dysfunction,[75–78] typical clinical features of the aged heart. It was shown that Wnt signaling is activated in type II lung epithelial cells and plays a causal role in the pathogenesis of lung fibrosis.[79–81] Likewise, Wnt signaling is upregulated in the α-smooth muscle actin–expressing activated fibroblasts in the kidney, and Wnt inhibition prevents fibrosis after renal injury.[82–84] These findings suggest that chronic activation of Wnt signaling induces transformation of fibroblasts into activated fibroblasts or myofibroblasts and contributes to cardiac fibrosis in the aged heart.

Wnt Activation in Vascular Cells

Vascular calcification is one of the features of age-related alterations in vascular structure,[85] and fate-mapping studies revealed that smooth muscle cells are the origin of osteochondrogenic precursors in arterial calcification.[86] It was shown that an osteogenic transcription factor Msx2 in adventitial myofibroblasts upregulates the expression of Wnt agonists and that these Wnt agonists act in a paracrine fashion on vascular smooth muscle cells and induce osteogenic differentiation of these cells by activating Wnt/β-catenin pathway.[87] It was also shown that lithium, a GSK-3β inhibitor and therefore an activator of Wnt signaling, induces endothelial cell senescence,[88] although this effect appears to be independent of GSK-3β inhibition by lithium.[89]

Wnt Activation in Cardiac Resident Stem Cells

In contrast to a classic view that the heart is a postmitotic organ, accumulating evidence suggests that the myocardium has the potential to regenerate and self-renew. It was previously shown by a genetic fate-mapping technique in mice that stem or progenitor cells contribute to the renewal of adult heart cells after injury but do not play a significant role in cardiomyocyte renewal during normal aging.[90] Subsequently, by measuring the integration of carbon 14 generated by nuclear bomb tests during the Cold War into cardiomyocytes, it was found that human heart has the capability to generate new cardiomyocytes, although with a low turnover rate.[91] Moreover, it was shown that mammalian myocardium contains small number of resident cardiac stem or progenitor cell population, characterized by the expression of specific markers. Those include c-kit$^+$ cells, Sca-1$^+$ cell, islet1$^+$ cells, and side-population cells.[92–97] It is therefore conceivable that resident stem/progenitor cells in the adult heart contribute to myocyte renewal during aging and after injury, although the situation may be slightly different in zebrafish heart, in which myocardial regeneration after injury occurs primarily through expansion of preexisting myocytes.[98,99]

Aging-associated decline in organ function is attributed, at least in part, to the aging of stem/progenitor cells in various tissues, including bone marrow, pancreas, and the brain.[100–102] In the heart, it was shown that the number of c-kit$^+$ cardiac stem cells was increased and that the percentage of stem cells that express a senescence marker p16 was higher in aged animals. Apoptotic cardiac stem cells were p16-positive, and the number of apoptotic stem cells was increased in aged hearts, resulting in a decline in the number of functional cardiac stem cells.[103,104] Of note, IGF signaling attenuated the aging-associated decline in stem cell function. Although this is inconsistent with the notion that the reduction in insulin/IGF signaling extends lifespan in multiple organisms, a similar observation was made in skeletal muscle expressing IGF-1 transgene.[105]

Whether Wnt activation in resident cardiac stem cells plays a causal role in aging-associated heart disorders is presently unknown. However, it was shown that genetic ablation of β-catenin in the second heart field results in the loss of second heart field-derived tissues and that stabilization of β-catenin in the second heart field results in massive accumulation of isl1$^+$ progenitors and inhibition of further differentiation of these cells into mature cardiomyocytes.[106–110] Thus, Wnt signaling promotes expansion of isl1$^+$ cardiac progenitor cells and subsequently inhibits further differentiation into mature cell types in the heart. This may partly explain why the number of cardiac stem/progenitor cells is increased, whereas the function of those cells to differentiate into mature cardiomyocytes is declined in the aged heart.[103,104]

Concluding Remarks

Our present knowledge on the role of Wnt signaling in aging-related malfunction of the heart is extremely limited. However, the observation that systemic factors in the serum of aged animals activate Wnt signaling and promote aging-related phenotypes at least in some tissues suggests that the aged heart is also a target of Wnt signaling. Further studies will be required to delineate whether aging-associated disorders in the heart are caused by enhanced Wnt signaling and whether inhibition of Wnt signaling is a novel therapeutic strategy for heart diseases in the elderly.

Sources of Funding

Work in our laboratory is supported by grants from the Ministry of Education, Culture, Sports, Science, and Technology (MEXT); Ministry of Health, Labour, and Welfare; and New Energy and Industrial Technology Development Organization (NEDO).

Disclosures

None.

References

1. Logan CY, Nusse R. The Wnt signaling pathway in development and disease. *Annu Rev Cell Dev Biol.* 2004;20:781–810.
2. Clevers H. Wnt/beta-catenin signaling in development and disease. *Cell.* 2006;127:469–480.
3. White BD, Nguyen NK, Moon RT. Wnt signaling: it gets more humorous with age. *Curr Biol.* 2007;17:R923–925.
4. Rao TP, Kuhl M. An updated overview on Wnt signaling pathways: a prelude for more. *Circ Res.* 2010;106:1798–1806.
5. Gessert S, Kuhl M. The multiple phases and faces of wnt signaling during cardiac differentiation and development. *Circ Res.* 2010;107:186–199.
6. Lakatta EG, Levy D. Arterial and cardiac aging: major shareholders in cardiovascular disease enterprises: Part II: the aging heart in health: links to heart disease. *Circulation.* 2003;107:346–354.
7. Campisi J, Kim SH, Lim CS, Rubio M. Cellular senescence, cancer and aging: the telomere connection. *Exp Gerontol.* 2001;36:1619–1637.
8. Campisi J. Senescent cells, tumor suppression, and organismal aging: good citizens, bad neighbors. *Cell.* 2005;120:513–522.
9. Park JI, Venteicher AS, Hong JY, Choi J, Jun S, Shkreli M, Chang W, Meng Z, Cheung P, Ji H, McLaughlin M, Veenstra TD, Nusse R,

McCrea PD, Artandi SE. Telomerase modulates Wnt signalling by association with target gene chromatin. *Nature*. 2009;460:66–72.
10. Richter T, von Zglinicki T. A continuous correlation between oxidative stress and telomere shortening in fibroblasts. *Exp Gerontol*. 2007;42:1039–1042.
11. von Zglinicki T. Role of oxidative stress in telomere length regulation and replicative senescence. *Ann N Y Acad Sci*. 2000;908:99–110.
12. von Zglinicki T, Pilger R, Sitte N. Accumulation of single-strand breaks is the major cause of telomere shortening in human fibroblasts. *Free Radic Biol Med*. 2000;28:64–74.
13. Serrano M, Lin AW, McCurrach ME, Beach D, Lowe SW. Oncogenic ras provokes premature cell senescence associated with accumulation of p53 and p16INK4a. *Cell*. 1997;88:593–602.
14. Bringold F, Serrano M. Tumor suppressors and oncogenes in cellular senescence. *Exp Gerontol*. 2000;35:317–329.
15. Itahana K, Dimri G, Campisi J. Regulation of cellular senescence by p53. *Eur J Biochem*. 2001;268:2784–2791.
16. Zhang H. Molecular signaling and genetic pathways of senescence: its role in tumorigenesis and aging. *J Cell Physiol*. 2007;210:567–574.
17. Muller M. Cellular senescence: molecular mechanisms, in vivo significance, and redox considerations. *Antioxid Redox Signal*. 2009;11:59–98.
18. Dimri G, Lee X, Basile G, Acosta M, Scott G, Roskelley C, Medrano EE, Linskens M, Rubelj I, Pereira-Smith O, Peacocke M, Campisi J. A biomarker that identifies senescent human cells in culture and in aging skin in vivo. *Proc Natl Acad Sci U S A*. 1995;92:9363–9367.
19. Finkel T, Serrano M, Blasco MA. The common biology of cancer and ageing. *Nature*. 2007;448:767–774.
20. Binet R, Ythier D, Robles AI, Collado M, Larrieu D, Fonti C, Brambilla E, Brambilla C, Serrano M, Harris CC, Pedeux R. WNT16B is a new marker of cellular senescence that regulates p53 activity and the phosphoinositide 3-kinase/AKT pathway. *Cancer Res*. 2009;69:9183–9191.
21. Minamino T, Miyauchi H, Yoshida T, Ishida Y, Yoshida H, Komuro I. Endothelial cell senescence in human atherosclerosis: role of telomere in endothelial dysfunction. *Circulation*. 2002;105:1541–1544.
22. Price JS, Waters JG, Darrah C, Pennington C, Edwards DR, Donell ST, Clark IM. The role of chondrocyte senescence in osteoarthritis. *Aging Cell*. 2002;1:57–65.
23. Minamino T, Yoshida T, Tateno K, Miyauchi H, Zou Y, Toko H, Komuro I. Ras induces vascular smooth muscle cell senescence and inflammation in human atherosclerosis. *Circulation*. 2003;108:2264–2269.
24. Sone H, Kagawa Y. Pancreatic beta cell senescence contributes to the pathogenesis of type 2 diabetes in high-fat diet-induced diabetic mice. *Diabetologia*. 2005;48:58–67.
25. Minamino T, Orimo M, Shimizu I, Kunieda T, Yokoyama M, Ito T, Nojima A, Nabetani A, Oike Y, Matsubara H, Ishikawa F, Komuro I. A crucial role for adipose tissue p53 in the regulation of insulin resistance. *Nat Med*. 2009;15:1082–1087.
26. Kirkwood TB, Austad SN. Why do we age? *Nature*. 2000;408:233–238.
27. Kenyon C, Chang J, Gensch E, Rudner A, Tabtiang R. A C. elegans mutant that lives twice as long as wild type. *Nature*. 1993;366:461–464.
28. Kenyon CJ. The genetics of ageing. *Nature*. 2010;464:504–512.
29. Tatar M, Bartke A, Antebi A. The endocrine regulation of aging by insulin-like signals. *Science*. 2003;299:1346–1351.
30. Kenyon C. The plasticity of aging: insights from long-lived mutants. *Cell*. 2005;120:449–460.
31. Kimura KD, Tissenbaum HA, Liu Y, Ruvkun G. daf-2, an insulin receptor-like gene that regulates longevity and diapause in Caenorhabditis elegans. *Science*. 1997;277:942–946.
32. Lin K, Dorman JB, Rodan A, Kenyon C. daf-16: an HNF-3/forkhead family member that can function to double the life-span of Caenorhabditis elegans. *Science*. 1997;278:1319–1322.
33. Ogg S, Paradis S, Gottlieb S, Patterson GI, Lee L, Tissenbaum HA, Ruvkun G. The Fork head transcription factor DAF-16 transduces insulin-like metabolic and longevity signals in C. elegans. *Nature*. 1997;389:994–999.
34. Morris JZ, Tissenbaum HA, Ruvkun G. A phosphatidylinositol-3-OH kinase family member regulating longevity and diapause in Caenorhabditis elegans. *Nature*. 1996;382:536–539.
35. Paradis S, Ruvkun G. Caenorhabditis elegans Akt/PKB transduces insulin receptor-like signals from AGE-1 PI3 kinase to the DAF-16 transcription factor. *Genes Dev*. 1998;12:2488–2498.
36. Tatar M, Kopelman A, Epstein D, Tu MP, Yin CM, Garofalo RS. A mutant Drosophila insulin receptor homolog that extends life-span and impairs neuroendocrine function. *Science*. 2001;292:107–110.
37. Clancy DJ, Gems D, Harshman LG, Oldham S, Stocker H, Hafen E, Leevers SJ, Partridge L. Extension of life-span by loss of CHICO, a Drosophila insulin receptor substrate protein. *Science*. 2001;292:104–106.
38. Tu MP, Epstein D, Tatar M. The demography of slow aging in male and female Drosophila mutant for the insulin-receptor substrate homologue chico. *Aging Cell*. 2002;1:75–80.
39. Holzenberger M, Dupont J, Ducos B, Leneuve P, Geloen A, Even PC, Cervera P, Le Bouc Y. IGF-1 receptor regulates lifespan and resistance to oxidative stress in mice. *Nature*. 2003;421:182–187.
40. Bluher M, Kahn BB, Kahn CR. Extended longevity in mice lacking the insulin receptor in adipose tissue. *Science*. 2003;299:572–574.
41. Taguchi A, Wartschow LM, White MF. Brain IRS2 signaling coordinates life span and nutrient homeostasis. *Science*. 2007;317:369–372.
42. Kops GJ, Dansen TB, Polderman PE, Saarloos I, Wirtz KW, Coffer PJ, Huang TT, Bos JL, Medema RH, Burgering BM. Forkhead transcription factor FOXO3a protects quiescent cells from oxidative stress. *Nature*. 2002;419:316–321.
43. Nemoto S, Finkel T. Redox regulation of forkhead proteins through a p66shc-dependent signaling pathway. *Science*. 2002;295:2450–2452.
44. Tran H, Brunet A, Grenier JM, Datta SR, Fornace AJ Jr, DiStefano PS, Chiang LW, Greenberg ME. DNA repair pathway stimulated by the forkhead transcription factor FOXO3a through the Gadd45 protein. *Science*. 2002;296:530–534.
45. Medema RH, Kops GJ, Bos JL, Burgering BM. AFX-like Forkhead transcription factors mediate cell-cycle regulation by Ras and PKB through p27kip1. *Nature*. 2000;404:782–787.
46. Orr WC, Sohal RS. Extension of life-span by overexpression of superoxide dismutase and catalase in Drosophila melanogaster. *Science*. 1994;263:1128–1130.
47. Schriner SE, Linford NJ, Martin GM, Treuting P, Ogburn CE, Emond M, Coskun PE, Ladiges W, Wolf N, Van Remmen H, Wallace DC, Rabinovitch PS. Extension of murine life span by overexpression of catalase targeted to mitochondria. *Science*. 2005;308:1909–1911.
48. Lee SS, Kennedy S, Tolonen AC, Ruvkun G. DAF-16 target genes that control C. elegans life-span and metabolism. *Science*. 2003;300:644–647.
49. Murphy CT, McCarroll SA, Bargmann CI, Fraser A, Kamath RS, Ahringer J, Li H, Kenyon C. Genes that act downstream of DAF-16 to influence the lifespan of Caenorhabditis elegans. *Nature*. 2003;424:277–283.
50. Ye X, Zerlanko B, Kennedy A, Banumathy G, Zhang R, Adams PD. Downregulation of Wnt signaling is a trigger for formation of facultative heterochromatin and onset of cell senescence in primary human cells. *Mol Cell*. 2007;27:183–196.
51. Liu H, Fergusson MM, Castilho RM, Liu J, Cao L, Chen J, Malide D, Rovira II, Schimel D, Kuo CJ, Gutkind JS, Hwang PM, Finkel T. Augmented Wnt signaling in a mammalian model of accelerated aging. *Science*. 2007;317:803–806.
52. Brack AS, Conboy MJ, Roy S, Lee M, Kuo CJ, Keller C, Rando TA. Increased Wnt signaling during aging alters muscle stem cell fate and increases fibrosis. *Science*. 2007;317:807–810.
53. Narita M, Nunez S, Heard E, Lin AW, Hearn SA, Spector DL, Hannon GJ, Lowe SW. Rb-mediated heterochromatin formation and silencing of E2F target genes during cellular senescence. *Cell*. 2003;113:703–716.
54. Zhang R, Poustovoitov MV, Ye X, Santos HA, Chen W, Daganzo SM, Erzberger JP, Serebriiskii IG, Canutescu AA, Dunbrack RL, Pehrson JR, Berger JM, Kaufman PD, Adams PD. Formation of MacroH2A-containing senescence-associated heterochromatin foci and senescence driven by ASF1a and HIRA. *Dev Cell*. 2005;8:19–30.
55. Kuro-o M, Matsumura Y, Aizawa H, Kawaguchi H, Suga T, Utsugi T, Ohyama Y, Kurabayashi M, Kaname T, Kume E, Iwasaki H, Iida A, Shiraki-Iida T, Nishikawa S, Nagai R, Nabeshima YI. Mutation of the mouse klotho gene leads to a syndrome resembling ageing. *Nature*. 1997;390:45–51.
56. Kuro-o M. Klotho and aging. *Biochim Biophys Acta*. 2009;1790:1049–1058.
57. Lanske B, Razzaque MS. Premature aging in klotho mutant mice: cause or consequence? *Ageing Res Rev*. 2007;6:73–79.
58. Conboy IM, Conboy MJ, Wagers AJ, Girma ER, Weissman IL, Rando TA. Rejuvenation of aged progenitor cells by exposure to a young systemic environment. *Nature*. 2005;433:760–764.
59. Kikuchi A, Yamamoto H, Kishida S. Multiplicity of the interactions of Wnt proteins and their receptors. *Cell Signal*. 2007;19:659–671.

60. Willert K, Brown JD, Danenberg E, Duncan AW, Weissman IL, Reya T, Yates JR III, Nusse R. Wnt proteins are lipid-modified and can act as stem cell growth factors. *Nature*. 2003;423:448–452.
61. Reya T, Duncan AW, Ailles L, Domen J, Scherer DC, Willert K, Hintz L, Nusse R, Weissman IL. A role for Wnt signalling in self-renewal of haematopoietic stem cells. *Nature*. 2003;423:409–414.
62. Kirstetter P, Anderson K, Porse BT, Jacobsen SE, Nerlov C. Activation of the canonical Wnt pathway leads to loss of hematopoietic stem cell repopulation and multilineage differentiation block. *Nat Immunol*. 2006; 7:1048–1056.
63. Scheller M, Huelsken J, Rosenbauer F, Taketo MM, Birchmeier W, Tenen DG, Leutz A. Hematopoietic stem cell and multilineage defects generated by constitutive beta-catenin activation. *Nat Immunol*. 2006;7: 1037–1047.
64. Essers MA, de Vries-Smits LM, Barker N, Polderman PE, Burgering BM, Korswagen HC. Functional interaction between beta-catenin and FOXO in oxidative stress signaling. *Science*. 2005;308:1181–1184.
65. Yoon JC, Ng A, Kim BH, Bianco A, Xavier RJ, Elledge SJ. Wnt signaling regulates mitochondrial physiology and insulin sensitivity. *Genes Dev*. 2010;24:1507–1518.
66. Polesskaya A, Seale P, Rudnicki MA. Wnt signaling induces the myogenic specification of resident CD45+ adult stem cells during muscle regeneration. *Cell*. 2003;113:841–852.
67. Ito M, Yang Z, Andl T, Cui C, Kim N, Millar SE, Cotsarelis G. Wnt-dependent de novo hair follicle regeneration in adult mouse skin after wounding. *Nature*. 2007;447:316–320.
68. Lakatta EG, Levy D. Arterial and cardiac aging: major shareholders in cardiovascular disease enterprises: Part I: aging arteries: a "set up" for vascular disease. *Circulation*. 2003;107:139–146.
69. Haq S, Michael A, Andreucci M, Bhattacharya K, Dotto P, Walters B, Woodgett J, Kilter H, Force T. Stabilization of beta-catenin by a Wnt-independent mechanism regulates cardiomyocyte growth. *Proc Natl Acad Sci U S A*. 2003;100:4610–4615.
70. Chen X, Shevtsov SP, Hsich E, Cui L, Haq S, Aronovitz M, Kerkela R, Molkentin JD, Liao R, Salomon RN, Patten R, Force T. The beta-catenin/T-cell factor/lymphocyte enhancer factor signaling pathway is required for normal and stress-induced cardiac hypertrophy. *Mol Cell Biol*. 2006;26:4462–4473.
71. Baurand A, Zelarayan L, Betney R, Gehrke C, Dunger S, Noack C, Busjahn A, Huelsken J, Taketo MM, Birchmeier W, Dietz R, Bergmann MW. Beta-catenin downregulation is required for adaptive cardiac remodeling. *Circ Res*. 2007;100:1353–1362.
72. Lombardi R, Dong J, Rodriguez G, Bell A, Leung TK, Schwartz RJ, Willerson JT, Brugada R, Marian AJ. Genetic fate mapping identifies second heart field progenitor cells as a source of adipocytes in arrhythmogenic right ventricular cardiomyopathy. *Circ Res*. 2009;104: 1076–1084.
73. Garcia-Gras E, Lombardi R, Giocondo MJ, Willerson JT, Schneider MD, Khoury DS, Marian AJ. Suppression of canonical Wnt/beta-catenin signaling by nuclear plakoglobin recapitulates phenotype of arrhythmogenic right ventricular cardiomyopathy. *J Clin Invest*. 2006;116: 2012–2021.
74. Gazoti Debessa CR, Mesiano Maifrino LB, Rodrigues de Souza R. Age related changes of the collagen network of the human heart. *Mech Ageing Dev*. 2001;122:1049–1058.
75. Burstein B, Nattel S. Atrial fibrosis: mechanisms and clinical relevance in atrial fibrillation. *J Am Coll Cardiol*. 2008;51:802–809.
76. Corradi D, Callegari S, Maestri R, Benussi S, Alfieri O. Structural remodeling in atrial fibrillation. *Nat Clin Pract Cardiovasc Med*. 2008; 5:782–796.
77. Burlew BS. Diastolic dysfunction in the elderly–the interstitial issue. *Am J Geriatr Cardiol*. 2004;13:29–38.
78. Ouzounian M, Lee DS, Liu PP. Diastolic heart failure: mechanisms and controversies. *Nat Clin Pract Cardiovasc Med*. 2008;5:375–386.
79. Chilosi M, Poletti V, Zamo A, Lestani M, Montagna L, Piccoli P, Pedron S, Bertaso M, Scarpa A, Murer B, Cancellieri A, Maestro R, Semenzato G, Doglioni C. Aberrant Wnt/beta-catenin pathway activation in idiopathic pulmonary fibrosis. *Am J Pathol*. 2003;162:1495–1502.
80. Konigshoff M, Balsara N, Pfaff EM, Kramer M, Chrobak I, Seeger W, Eickelberg O. Functional Wnt signaling is increased in idiopathic pulmonary fibrosis. *PLoS One*. 2008;3:e2142.
81. Konigshoff M, Kramer M, Balsara N, Wilhelm J, Amarie OV, Jahn A, Rose F, Fink L, Seeger W, Schaefer L, Gunther A, Eickelberg O. WNT1-inducible signaling protein-1 mediates pulmonary fibrosis in mice and is upregulated in humans with idiopathic pulmonary fibrosis. *J Clin Invest*. 2009;119:772–787.
82. Surendran K, McCaul SP, Simon TC. A role for Wnt-4 in renal fibrosis. *Am J Physiol Renal Physiol*. 2002;282:F431–F441.
83. Surendran K, Schiavi S, Hruska KA. Wnt-dependent beta-catenin signaling is activated after unilateral ureteral obstruction, and recombinant secreted frizzled-related protein 4 alters the progression of renal fibrosis. *J Am Soc Nephrol*. 2005;16:2373–2384.
84. He W, Dai C, Li Y, Zeng G, Monga SP, Liu Y. Wnt/beta-catenin signaling promotes renal interstitial fibrosis. *J Am Soc Nephrol*. 2009; 20:765–776.
85. Abedin M, Tintut Y, Demer LL. Vascular calcification: mechanisms and clinical ramifications. *Arterioscler Thromb Vasc Biol*. 2004;24: 1161–1170.
86. Speer MY, Yang HY, Brabb T, Leaf E, Look A, Lin WL, Frutkin A, Dichek D, Giachelli CM. Smooth muscle cells give rise to osteochondrogenic precursors and chondrocytes in calcifying arteries. *Circ Res*. 2009;104:733–741.
87. Shao JS, Cheng SL, Pingsterhaus JM, Charlton-Kachigian N, Loewy AP, Towler DA. Msx2 promotes cardiovascular calcification by activating paracrine Wnt signals. *J Clin Invest*. 2005;115:1210–1220.
88. Mao CD, Hoang P, DiCorleto PE. Lithium inhibits cell cycle progression and induces stabilization of p53 in bovine aortic endothelial cells. *J Biol Chem*. 2001;276:26180–26188.
89. Struewing IT, Durham SN, Barnett CD, Mao CD. Enhanced endothelial cell senescence by lithium-induced matrix metalloproteinase-1 expression. *J Biol Chem*. 2009;284:17595–17606.
90. Hsieh PC, Segers VF, Davis ME, MacGillivray C, Gannon J, Molkentin JD, Robbins J, Lee RT. Evidence from a genetic fate-mapping study that stem cells refresh adult mammalian cardiomyocytes after injury. *Nat Med*. 2007;13:970–974.
91. Bergmann O, Bhardwaj RD, Bernard S, Zdunek S, Barnabe-Heider F, Walsh S, Zupicich J, Alkass K, Buchholz BA, Druid H, Jovinge S, Frisen J. Evidence for cardiomyocyte renewal in humans. *Science*. 2009;324:98–102.
92. Beltrami AP, Barlucchi L, Torella D, Baker M, Limana F, Chimenti S, Kasahara H, Rota M, Musso E, Urbanek K, Leri A, Kajstura J, Nadal-Ginard B, Anversa P. Adult cardiac stem cells are multipotent and support myocardial regeneration. *Cell*. 2003;114:763–776.
93. Oh H, Bradfute SB, Gallardo TD, Nakamura T, Gaussin V, Mishina Y, Pocius J, Michael LH, Behringer RR, Garry DJ, Entman ML, Schneider MD. Cardiac progenitor cells from adult myocardium: homing, differentiation, and fusion after infarction. *Proc Natl Acad Sci U S A*. 2003; 100:12313–12318.
94. Matsuura K, Nagai T, Nishigaki N, Oyama T, Nishi J, Wada H, Sano M, Toko H, Akazawa H, Sato T, Nakaya H, Kasanuki H, Komuro I. Adult cardiac Sca-1-positive cells differentiate into beating cardiomyocytes. *J Biol Chem*. 2004;279:11384–11391.
95. Laugwitz KL, Moretti A, Lam J, Gruber P, Chen Y, Woodard S, Lin LZ, Cai CL, Lu MM, Reth M, Platoshyn O, Yuan JX, Evans S, Chien KR. Postnatal isl1+ cardioblasts enter fully differentiated cardiomyocyte lineages. *Nature*. 2005;433:647–653.
96. Martin CM, Meeson AP, Robertson SM, Hawke TJ, Richardson JA, Bates S, Goetsch SC, Gallardo TD, Garry DJ. Persistent expression of the ATP-binding cassette transporter, Abcg2, identifies cardiac SP cells in the developing and adult heart. *Dev Biol*. 2004;265:262–275.
97. Oyama T, Nagai T, Wada H, Naito AT, Matsuura K, Iwanaga K, Takahashi T, Goto M, Mikami Y, Yasuda N, Akazawa H, Uezumi A, Takeda S, Komuro I. Cardiac side population cells have a potential to migrate and differentiate into cardiomyocytes in vitro and in vivo. *J Cell Biol*. 2007;176:329–341.
98. Jopling C, Sleep E, Raya M, Marti M, Raya A, Belmonte JC. Zebrafish heart regeneration occurs by cardiomyocyte dedifferentiation and proliferation. *Nature*. 2010;464:606–609.
99. Kikuchi K, Holdway JE, Werdich AA, Anderson RM, Fang Y, Egnaczyk GF, Evans T, Macrae CA, Stainier DY, Poss KD. Primary contribution to zebrafish heart regeneration by gata4(+) cardiomyocytes. *Nature*. 2010;464:601–605.
100. Janzen V, Forkert R, Fleming HE, Saito Y, Waring MT, Dombkowski DM, Cheng T, DePinho RA, Sharpless NE, Scadden DT. Stem-cell ageing modified by the cyclin-dependent kinase inhibitor p16INK4a. *Nature*. 2006;443:421–426.
101. Molofsky AV, Slutsky SG, Joseph NM, He S, Pardal R, Krishnamurthy J, Sharpless NE, Morrison SJ. Increasing p16INK4a expression

decreases forebrain progenitors and neurogenesis during ageing. *Nature*. 2006;443:448–452.
102. Krishnamurthy J, Ramsey MR, Ligon KL, Torrice C, Koh A, Bonner-Weir S, Sharpless NE. p16INK4a induces an age-dependent decline in islet regenerative potential. *Nature*. 2006;443:453–457.
103. Torella D, Rota M, Nurzynska D, Musso E, Monsen A, Shiraishi I, Zias E, Walsh K, Rosenzweig A, Sussman MA, Urbanek K, Nadal-Ginard B, Kajstura J, Anversa P, Leri A. Cardiac stem cell and myocyte aging, heart failure, and insulin-like growth factor-1 overexpression. *Circ Res*. 2004;94:514–524.
104. Gonzalez A, Rota M, Nurzynska D, Misao Y, Tillmanns J, Ojaimi C, Padin-Iruegas ME, Muller P, Esposito G, Bearzi C, Vitale S, Dawn B, Sanganalmath SK, Baker M, Hintze TH, Bolli R, Urbanek K, Hosoda T, Anversa P, Kajstura J, Leri A. Activation of cardiac progenitor cells reverses the failing heart senescent phenotype and prolongs lifespan. *Circ Res*. 2008;102:597–606.
105. Musaro A, McCullagh K, Paul A, Houghton L, Dobrowolny G, Molinaro M, Barton ER, Sweeney HL, Rosenthal N. Localized Igf-1 transgene expression sustains hypertrophy and regeneration in senescent skeletal muscle. *Nat Genet*. 2001;27:195–200.
106. Ai D, Fu X, Wang J, Lu MF, Chen L, Baldini A, Klein WH, Martin JF. Canonical Wnt signaling functions in second heart field to promote right ventricular growth. *Proc Natl Acad Sci U S A*. 2007;104:9319–9324.
107. Cohen ED, Wang Z, Lepore JJ, Lu MM, Taketo MM, Epstein DJ, Morrisey EE. Wnt/beta-catenin signaling promotes expansion of Isl-1-positive cardiac progenitor cells through regulation of FGF signaling. *J Clin Invest*. 2007;117:1794–1804.
108. Kwon C, Arnold J, Hsiao EC, Taketo MM, Conklin BR, Srivastava D. Canonical Wnt signaling is a positive regulator of mammalian cardiac progenitors. *Proc Natl Acad Sci U S A*. 2007;104:10894–10899.
109. Lin L, Cui L, Zhou W, Dufort D, Zhang X, Cai CL, Bu L, Yang L, Martin J, Kemler R, Rosenfeld MG, Chen J, Evans SM. Beta-catenin directly regulates Islet1 expression in cardiovascular progenitors and is required for multiple aspects of cardiogenesis. *Proc Natl Acad Sci U S A*. 2007;104:9313–9318.
110. Qyang Y, Martin-Puig S, Chiravuri M, Chen S, Xu H, Bu L, Jiang X, Lin L, Granger A, Moretti A, Caron L, Wu X, Clarke J, Taketo MM, Laugwitz KL, Moon RT, Gruber P, Evans SM, Ding S, Chien KR. The renewal and differentiation of Isl1+ cardiovascular progenitors are controlled by a Wnt/beta-catenin pathway. *Cell Stem Cell*. 2007;1:165–179.

Journal of Molecular and Cellular Cardiology 49 (2010) 972–983

Contents lists available at ScienceDirect

Journal of Molecular and Cellular Cardiology

journal homepage: www.elsevier.com/locate/yjmcc

Original article

Implantation of cardiac progenitor cells using self-assembling peptide improves cardiac function after myocardial infarction

Masakuni Tokunaga [a,1], Mei-Lan Liu [a,1], Toshio Nagai [a], Koji Iwanaga [a], Katsuhisa Matsuura [b], Toshinao Takahashi [a], Masato Kanda [a], Naomichi Kondo [a], Pin Wang [a], Atsuhiko T. Naito [a], Issei Komuro [a,c,*]

[a] Department of Cardiovascular Science and Medicine, Chiba University Graduate School of Medicine, 1-8-1 Inohana, Chuo-ku, Chiba 260-8670, Japan
[b] Department of Cardiology and Institute of Advanced Biomedical Engineering and Science, Tokyo Women's Medical University, 8-1 Kawada-cho, Shinjuku-ku, Tokyo 162-8666, Japan
[c] Department of Cardiovascular Medicine, Osaka University Graduate School of Medicine, 2-2 Yamadaoka, Suita, Osaka 565-0871, Japan

ARTICLE INFO

Article history:
Received 18 February 2010
Received in revised form 20 August 2010
Accepted 15 September 2010
Available online 24 September 2010

Keywords:
Cardiac progenitor cells
Stem cell antigen-1
Cell transplantation
Self-assembling nanopeptides
Myocardial infarction

ABSTRACT

Implantation of various types of cells into the heart has been reported to be effective for heart failure, however, it is unknown what kinds of cells are most suitable for myocardial repair. To examine which types of cells are most effective, we injected cell–Puramatrix™ (PM) complex into the border area and overlaid the cell–PM patch on the myocardial infarction (MI) area. We compared cardiac morphology and function at 2 weeks after transplantation. Among clonal stem cell antigen-1 positive cardiac progenitors with PM (cSca-1/PM), bone marrow mononuclear cells with PM (BM/PM), skeletal myoblasts with PM (SM/PM), adipose tissue-derived mesenchymal cells with PM (AMC/PM), PM alone (PM), and non-treated MI group (MI), the infarct area of cSca-1/PM was smaller than that of BM/PM, SM/PM, PM and MI. cSca-1/PM and AMC/PM attenuated ventricular enlargement and restored cardiac function in comparison with MI. Capillary density in the infarct area of cSca-1/PM was higher than that of other five groups. The percentage of TUNEL positive cardiomyocytes in the infarct area of cSca-1/PM was lower than that of MI and PM. cSca-1 secreted VEGF and some of them differentiated into cardiomyocytes and vascular smooth muscle cells. These results suggest that transplantation of cSca-1/PM most effectively prevents cardiac remodeling and dysfunction through angiogenesis, inhibition of apoptosis and myocardial regeneration.

1. Introduction

Cell therapy has been expected to be a new therapy for severe heart failure [1]. Various types of cell sources such as skeletal myoblasts, bone marrow mononuclear cells and mesenchymal stem cells have been examined in both basic and clinical studies [2]. Although there have been reports showing that transplanted cells improve the function of ischemic heart, the effects of cell therapy are variable among the clinical trials and it is still unknown how they show beneficial effects and what kinds of cells are suitable for myocardial repair [3,4]. A low rate of engraftment of transplanted cells, which stem from leakage and wash out during injections and massive death of cells, hampers the efficiency of cell transplantation within the host tissue [5,6]. Biological scaffolds are expected to circumvent the loss of grafted cells as they confer the three-dimensional microenvironment for the cells and support their survival, proliferation and function [7]. Many kinds of scaffolds have been designed at present; however, there are many unsolved issues in terms of their matching to engrafted cells, compatibility with host tissue, and clinical safety.

Self-assembling nanopeptides consist of alternating hydrophilic and hydrophobic amino acid residues that can adopt ß-sheet structures and forms a stable three-dimensional hydrogel consisting of >99.5% water depending upon pH, salt, and time [8]. The hydrogel has been shown to promote cell survival, proliferation and differentiation of many different cell types in culture, including neural stem cells [9], osteocytes [10], and endothelial cells [11]. When self-assembling peptides are injected into the tissue, they form a nanofiber network, which confers three-dimensional microenvironments for the endogenous cells, leading to angiogenesis and neuronal axon regeneration [12,13]. Self-assembling nanopeptides have been reported to be useful for protein delivery system. Charged assembled peptides can directly bind to platelet-derived growth factor (PDGF) or can be designed to conjugate with insulin-like growth factor-1 (IGF-1). Injection of PDGF or IGF-1 with self-assembling peptides after myocardial infarction has been reported to decrease infarct size, improve cardiac function and increase survival of co-transplanted neonatal rat cardiomyocytes [14,15]. These findings suggest that self-assembling nanopeptides are effective as a biological scaffold for various types of cells, which are currently investigated as candidates for transplantation to the diseased heart.

* Corresponding author. Department of Cardiovascular Science and Medicine, Chiba University Graduate School of Medicine, 1-8-1 Inohana, Chuo-ku, Chiba 260-8670, Japan. Tel.: +81 43 226 2097; fax: +81 43 226-2557.
E-mail address: komuro-tky@umin.ac.jp (I. Komuro).
[1] Masakuni Tokunaga and Mei-Lan Liu equally contributed to this work.

0022-2828/$ – see front matter © 2010 Elsevier Ltd. All rights reserved.
doi:10.1016/j.yjmcc.2010.09.015

In this manuscript, we transplanted self-assembling nanopeptides with various types of cells such as bone marrow mononuclear cells (BM), skeletal myoblasts (SM), adipose tissue-derived mesenchymal cells (AMC) or clonal stem cell antigen-1 positive cardiac progenitors (cSca-1), into mouse hearts after producing myocardial infarction (MI) and determined the most effective cell sources to reduce infarct size and prevent cardiac dysfunction. In addition, we examined the potential mechanisms of beneficial effects of a complex of cardiac progenitors and self-assembling nanopetides.

2. Material and methods

2.1. Animals

Wild mice (C57Bl/6J, 10–12 weeks) were purchased from Japan SLC (Shizuoka, Japan). Adult GFP transgenic mice [16] were purchased from Japan SLC, Japan. All protocols were approved by the Institutional Animal Care and Use Committee of Chiba University Graduate School of Medicine and the Japanese Government Animal Protection and Management Law (no. 105).

2.2. Preparation of cells

cSca-1 are a cell line of cardiac progenitor cells established from adult mouse heart Sca-1 positive cells as described previously [17,18]. AMC were isolated from adult mice as described previously [19] with a few modifications. Briefly, white adipose tissues were digested at 37 °C in PBS with 2.5 mg/ml of dispase (Invitrogen, Carlsbad) for 45 min. After filtration through 25-μm filters and centrifugation, isolated AMC were suspended in Iscove's modified Dulbecco's medium (IMDM, Invitrogen) supplemented with 10% fetal bovine serum (FBS) and penicillin/streptomycin, and cultured on 1% gelatin-coated dishes. AMC after passages 3 to 5 were used. SM were isolated from the hind limbs of adult mice as described previously [20]. In brief, minced muscle tissues were digested in 0.05% trypsin-EDTA and cultured in F-10 medium (Invitrogen) with 20% horse serum and 2.5 ng/ml basic fibroblast growth factor (bFGF, Promega Madison) for 4 days. SM were expanded in the medium with 20% FBS and used within 2 to 3 passages. BM were harvested from adult mice. Mononuclear cells were subsequently separated using Histopaque 1083 (Sigma-Aldrich Japan, Tokyo, Japan) and suspended in IMDM supplemented with 10% FBS and subsequently used for cell transplantation. To obtain the growth curve of cSca-1, AMC and SM, the number of cultured cells was measured by Countess (Life Technology Corp.) at an appropriate time period. Green fluorescence protein (GFP)- and red fluorescence protein (RFP)-expressing retroviral stocks were generated as described previously [21]. cSca-1 were infected with the GFP- or RFP-expressing retroviral vector. Infected cells were selected for growth in the presence of 500 μg/ml of neomycin (Sigma-Aldrich) for 2 weeks. The efficiency of transfection of GFP and RFP was >95%.

2.3. Animal surgery and cell transplantation

The mice were anesthetized by intra-peritoneal injection of 50 mg/kg of sodium pentobarbital and ventilated with a volume-regulated respirator. MI was produced by ligation of the left anterior descending artery with a 10-0 Prolene suture. Puramatrix™ (PM; peptide sequence AcNRADARADARADARADA-CNH2, RAD16-I) was kindly provided by 3-D Matrix, Ltd. (Tokyo, Japan). PM was dissolved in 295 mM sucrose solution (1% W/V) and sonicated before use [22]. The cells were suspended in 295 mM sucrose solution (1% W/V) and mixed with 1% PM/sucrose solution at the ratio of 1:1 or 1:9. Thus the final concentration of PM in the cell mixture was 0.1% or 0.5%, respectively. Within 5 min after ligation of the left anterior descending artery, 10 μl of 0.1% PM–cell mixture containing 2×10^4 cells was directly injected into the border zone of the myocardium two times (Supplemental Figs. 1A and C). Subsequently, 20 μl of 0.5% PM–cell mixture containing 2×10^4 cells was disseminated onto the surface of the infarct area (Supplemental Figs. 1B and C). PM polymerized within minutes when it encountered neutral body fluid, which contains salt (Supplemental Fig. 1D). When cSca-1 were transplanted without PM, 10 μl of 295 mM sucrose solution containing 2×10^4 of cSca-1 cells was injected directly into the border zone of the myocardium two times. To neutralize the vascular endothelial growth factor (VEGF), cSca-1/PM with 100 ng/ml of goat anti-mouse VEGF antibody (R&D systems) or normal goat IgG (R&D systems) were injected.

2.4. Morphological examination and infarct size measurement

The hearts were fixed in 10% PBS buffered formalin (Wako, Osaka Japan), embedded in paraffin and several transverse sections (4 μm) were collected every 0.4 mm from the apex, mid and base. Fibrous infarct area was detected visually by Masson Trichrome staining. The lengths of scar and of noninfarcted muscle for both the endocardial and epicardial surfaces of each histological section were measured. The final infarct size was expressed in percentage as the average of the endocardial and epicardial lengths of scar of surface circumferences times one hundred [23]. For area at risk (AAR) and infarct size (INF) assessment, mice were anesthetized and the left anterior descending artery was re-occluded at 2 weeks after transplantation. Evan's blue dye (2.5%, Wako Japan) was injected from left ventricular apex to delineate the in vivo AAR. The heart was rapidly excised, frozen and sectioned into 2 mm transverse sections from the apex to base. Following defrosting, the slices were incubated at 37 °C with 2% triphenylte-trazolium chloride in phosphate buffer (pH 7.4) for 30 min, fixed n 10% formaldehyde solution and photographed with a digital camera (Leica Germany). AAR and INF were expressed as percentage of ventricle surface (AAR/LV) and AAR (INF/AAR), respectively.

2.5. Echocardiography

Echocardiography in spontaneous breathing mice was performed using a Vevo770 (Visual Sonics, Toronto, Canada) with a 25-MHz imaging transducer. Two-dimensional images and M-mode tracing were recorded from the parasternal long axis view at midpapillary level to determine the left ventricular internal diastole diameter (LVIDD) and left ventricular internal systolic diameter (LVISD). LV fractional shortening (FS) was calculated as $\%FS = [(LVIDD - LVISD)/LVIDD]\times 100$.

2.6. Immunohistochemistry and cytochemistry

Paraffin-embedded heart tissues were sectioned at 4 μm thickness and stained overnight at 4 °C with anti-von-Willebrand factor (anti-vWF) (DAKO, Kyoto, Japan) and anti-alpha-smooth muscle cell actin (anti-SMA, clone 1A4; Sigma-Aldrich). Detection of antibodies was performed by using VECSTATIN ABC kit (Vector Laboratories Inc. CA) according to the manufacturer's instructions. Nuclei were stained with hematoxylin. For the detection of TUNEL positive cardiomyocytes and endothelial cells, fresh frozen sections (4 μm) were fixed with acetone for 5 min at 4 °C and then TUNEL staining was performed by using in situ Apoptosis Detection kit (TAKARA BIO Inc. Sigma, Japan) or TMR red (Roche Diagnostics Suisse) according to the manufacturer's instructions. The sections were subsequently stained with anti-alpha-sarcomeric actinin (anti-SA) (clone EA-53; Sigma-Aldrich) and anti-CD31 (clone MEC 13.3; BD Biosciences CA) primary antibodies and then with FITC or Cy3 conjugated secondary antibodies (Jackson Immuno Research Laboratory, MO). For the detection of transplanted GFP- or RFP-expressing cSca-1, fresh frozen sections were fixed with 4% paraformaldehyde and double-stained with anti-

GFP or anti-RFP (MBL, Aichi, Japan) antibodies in combination with anti-SMA or anti-SA actinin antibodies. Anti-GFP antibody was detected with FITC conjugated anti-rabbit IgG, and subsequently enhanced with Alexa Fluor 488 conjugated anti-FITC antibody (Molecular Probes, Invitrogen CA). Other primary antibodies were detected with appropriate fluorescent conjugated secondary antibodies (Jackson Immuno Research Laboratory). Nuclei were stained with TOPRO3 (Molecular Probes) or Hochst33342 (Sigma-Aldrich). The frequency of transplanted cells was expressed in percentage of the number of GFP-expressing cells divided by the total number of nuclei per field. The percentage of myoblasts in cultured SM was examined by immunocytochemical method by using anti-SA actinin antibodies as previously described [21]. All of the images of cells and tissues were taken by laser confocal microscopy (Radiance 2000 Bio-Rad Hercules CA, FV10i Olympus Tokyo Japan), or fluorescent microscopy (Axiovert 200, Zeiss, Germany).

2.7. Flow cytometric analysis

The immunostaining methods have been previously described [17]. The percentage of cells expressing each cell surface antigen was analyzed with an EPICS ALTRA flow cytometer using EXPO32 software, version 1.2 (Beckman Coulter, Inc. CA). PE anti-mouse CD34, PE anti-mouse CD45 and PE rat IgG2a were purchased from BD Biosciences. PE anti-mouse CD31, PE anti-mouse Sca-1, PE anti-mouse CD105, PE anti-mouse CD90, PE anti-mouse c-kit and PE rat IgG2b were purchased from eBioscience, Inc. CA.

2.8. Detection of cytokines

cSca-1 and AMC (1.0×10^6) were seeded on 10-cm dishes. After incubation for 12 h in medium supplemented with 10% FBS, cells were washed with PBS thoroughly three times, and incubated with a serum-depleted medium. After 24 h, supernatant was collected and contaminated cells were removed by centrifugation at 1000 rpm. The supernatant of a heart tissue sample was prepared according to the manufacturer's instructions. The concentration of vascular endothelial growth factor (VEGF), bFGF and platelet-derived growth factor-bb (PDGF-bb) was simultaneously evaluated using multiplex bead-based sandwich immunoassay kits (Bio-Rad Laboratories, CA), following the manufacturer's instructions. Briefly, the supernatant (50 μl/well) or standards (50 μl/well) were incubated with 50 μl of pre-mixed bead sets into the wells of a pre-wet 96 well plate. After incubation and washing, 25 μl of fluorescent detection antibody mixture was added for 30 min and then the samples were washed and resuspended in an assay buffer. The formation of different sandwich immunocomplexes on distinct bead sets was measured and quantified using the Bio-Plex Protein Array System (Bio-Rad Laboratories).

2.9. Statistical analysis

Data are shown as means ± SD. Multiple group comparison was performed by one-way ANOVA followed by the Bonferroni procedure for comparison of means. Comparison of the means of two samples was performed by t-test. A value of $p<0.05$ was considered significant.

3. Results

3.1. Profile of transplanted cells

The population doubling time of cSca-1, AMC and SM was 1.6, 3.3 and 2.0 days, respectively. Log phase of growth period was identified from the growth curve of cSca-1, AMC and SM (Supplemental Fig. 1E). The growth rate constant of cSca-1, AMC and SM was 0.19, 0.06 and 0.03/h, respectively. BM cultured in IMDM did not proliferate during observation. The percentage of SA actinin positive myoblasts was ~23% in cultured SM (Supplemental Fig. 1F). The analysis of cell surface proteins revealed that hematopoietic and endothelial lineage markers, such as c-kit, CD45 and CD31 were positive in BM but not detectable in cSca-1, AMC and SM (Supplemental Figs. 2A and B, Supplemental Figs. 3A and B). CD90 and CD105, which have been reported to be mesenchymal stem cell markers were expressed in AMC and SM but quite low in cSca-1 and BM [24]. Almost 100% of cSca-1 and 30 to 40% of AMC and SM expressed Sca-1. Expression of CD34 was observed in cSca-1 and BM but not in AMC and SM.

3.2. Transplantation of cSca-1 with PM attenuates the expansion of infarct size

We embedded various types of cells such as cSca-1, BM, SM, or AMC in the PM before gelation. These cell/PM complexes were injected into the border area of MI and disseminated over the area of MI. At 2 weeks after transplantation, Masson's trichrome-stained myocardial images revealed that the infarct area of the heart treated with cSca-1/PM (Fig. 1F) was remarkably smaller than that of non-treated MI (Fig. 1A), the heart treated with PM (Fig. 1B), BM/PM (Fig. 1C), SM/PM (Fig. 1D) and AMC/PM (Fig. 1E). Averaged infarct area was 38.6 ± 11.9% in cSca-1/PM-treated ($n=19$) hearts, 57.4 ± 9.9% in non-treated MI ($n=12$), 55.9 ± 13.1% in PM-treated ($n=17$), 55.2 ± 6.0% in BM/PM-treated ($n=7$), 57.9 ± 7.4% in SM/PM-treated ($n=6$), and 51.3 ± 10.5% in AMC/PM-treated ($n=8$) hearts (cSca-1/PM-treated vs. non-treated MI, PM-treated and SM/PM-treated hearts; $p<0.01$, cSca-1/PM-treated vs. BM/PM-treated hearts; $p<0.05$, Fig. 1G). When cSca-1 were directly injected without PM, the averaged infarct area was 53.9 ± 7.4% ($n=9$) (Supplemental Fig. 1H), which is comparable with that of non-treated MI (Supplemental Fig. 1I) and significantly larger than that of cSca-1/PM-treated hearts (Supplemental Fig. 1G, cSca-1/PM-treated vs. cSca-1; $p<0.01$, Supplemental Fig. 1J). No significant difference was observed in age, body weight (BW), heart weight (HW) and HW to BW ratio among the groups subjected to quantification of the infarct area (Supplemental Table A). To confirm whether cSca-1/PM reduce the infarct size irrespective of the size of initial ischemic area, we examined AAR and INF. Representative images of AAR and INF staining for PM- and cSca-1/PM-treated mice at 2 weeks after MI were presented in Supplemental Figs. 4A and B, respectively. AAR/LV was 52.6 ± 15.9% and 51.5 ± 10.0% in PM- and cSca-1/PM-treated mice, respectively (Supplemental Fig. 4C). INF/AAR was 84.9 ± 11.5% and 61.5 ± 9.31% in PM- and cSca-1/PM-treated mice, respectively (cSca-1/PM-treated vs. PM-treated; $p\leq0.05$, Supplemental Fig. 4D). Despite similar-sized AAR, cSca-1/PM-treated mice showed a significantly smaller INF/AAR in comparison with PM-treated mice. These findings suggest that cSca-1 are most effective to prevent cardiac remodeling after MI, when injected in PM.

3.3. Transplantation of cSca-1 with PM attenuates left ventricular remodeling and systolic dysfunction

Echocardiographic measurement of the hearts at 2 weeks after cell transplantation was summarized in Table 1. LVIDD of cSca-1/PM-treated hearts was significantly smaller than that of other six groups. LVISD of cSca-1/PM-treated and AMC/PM-treated hearts was significantly smaller than that of other five groups. These reductions were associated with a significantly greater value of %FS in cSca-1/PM-treated and AMC/PM-treated hearts. The hearts injected with cSca-1 without PM did not show any functional improvement. There was no significant deference in heart rate (HR) among the 7 groups at 2 weeks after cell transplantation (Table 1). When blood pressure (BP) and HR was examined before and after cell transplantation, there was no significant difference in BP and HR between cSca-1 and other groups (Supplemental Table B). These findings suggest that cSca-1/PM attenuate both left ventricular enlargement and contractile dysfunction without a significant change in blood pressure and heart rate.

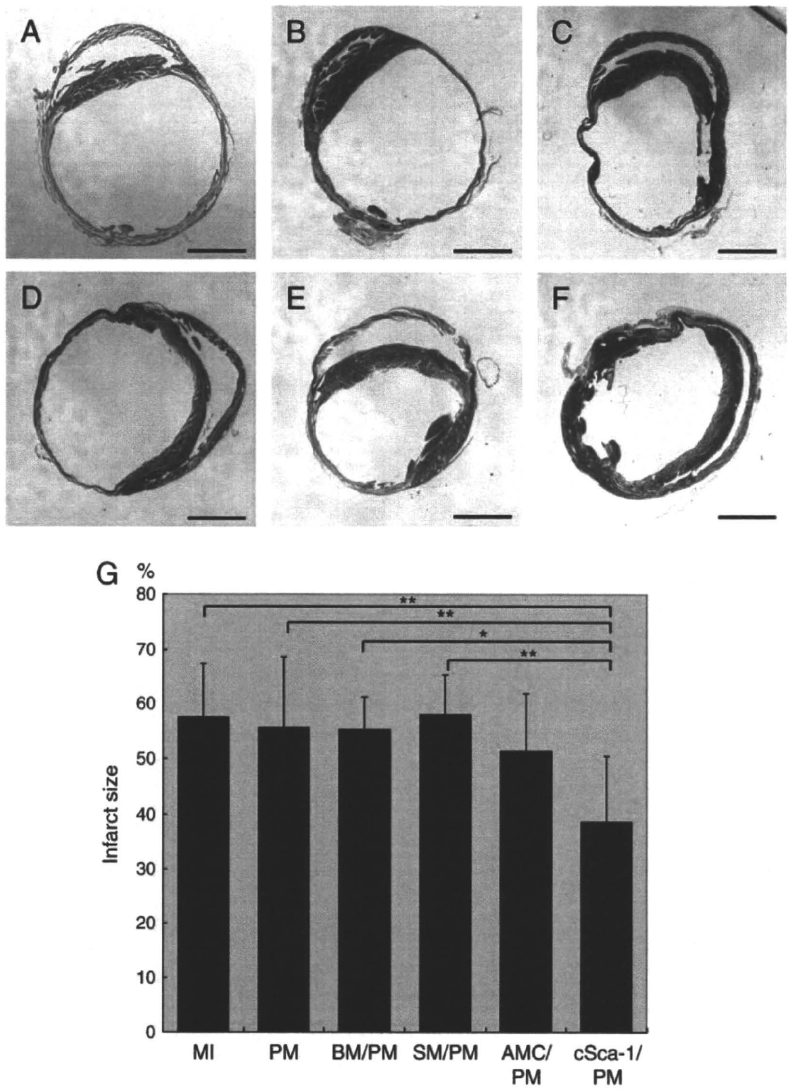

Fig. 1. Transplantation of cSca-1 with PM attenuates the expansion of infarct size. Representative Masson's trichrome-stained myocardial sections from non-treated MI (A), PM-treated (B), BM/PM-treated (C), SM/PM-treated (D), AMC/PM-treated (E) and cSca-1/PM-treated (F) hearts. Bars are 2.5 mm. (G): Quantification of the infarct size 14 days after transplantation. Data are mean ± SD. *p<0.05 cSca-1/PM-treated vs. BM/PM-treated group; **p<0.01 cSca-1/PM-treated vs. non-treated MI, PM-treated, SM/PM-treated and AMC/PM-treated group. Backgrounds of mice in each group are shown in Supplemental Table A.

3.4. Transplantation of cSca-1 with PM increases the number of vWF-positive capillary in infarct area

To elucidate the mechanisms of the beneficial effects of transplantation of cSca-1/PM complex, we first examined the effects of transplantation on neovascularization in post-MI hearts. At 2 weeks after transplantation, immunohistochemical staining for vWF indicated that more vWF-positive capillaries exist in the infarct area of cSca-1/PM-treated heart (Fig. 2F) in comparison with non-treated MI (Fig. 2A), PM-treated (Fig. 2B), BM/PM-treated (Fig. 2C), SM/PM-treated (Fig. 2D) and AMC/PM-treated (Fig. 2E) hearts. The number of vWF-positive capillaries per mm^2 was 23.4 ± 7.7 in non-treated MI

Table 1
Echocardiographic measurement of hearts 2 weeks after cell transplantation.

Parameter	MI	PM	BM/PM	SM/PM	AMC/PM	cSca-1/PM	cSca-1
n	13	20	8	11	16	24	14
Age (week)	13.5 ± 2.1	13.0 ± 1.8	12.8 ± 1.5	14.1 ± 1.1	13.8 ± 0.7	13.6 ± 1.0	14.0 ± 2.3
BW (g)	24.8 ± 2.2	25.1 ± 2.0	24.7 ± 1.3	24.9 ± 2.0	25.0 ± 1.6	25.4 ± 1.4	26.5 ± 2.4
HW (mg)	172 ± 46	172 ± 39	175 ± 25	181 ± 37	155 ± 26	168 ± 38	177 ± 32
HW/BW (mg/g)	7.0 ± 1.9	6.8 ± 1.4	7.1 ± 1.2	7.3 ± 1.5	6.2 ± 1.0	6.6 ± 1.4	6.7 ± 1.0
HR (min^{-1})	697 ± 55	711 ± 40	729 ± 50	712 ± 48	700 ± 60	689 ± 42	689 ± 61
LVIDD (mm)	5.9 ± 0.6	5.5 ± 0.7	5.8 ± 0.6	5.3 ± 1.0	5.0 ± 1.0	4.8 ± 0.9[a]	5.0 ± 1.1
LVISD (mm)	5.5 ± 0.6	4.9 ± 0.9	5.2 ± 0.8	4.7 ± 1.2	4.3 ± 1.3[a]	4.1 ± 1.1[a]	4.4 ± 1.3
%FS	6.5 ± 2.3	11 ± 5.5	9.6 ± 4.6	12.2 ± 8.2	16.5 ± 11[a]	16.2 ± 11[a]	14.8 ± 9.4

[a] p<0.05 in comparison with MI.

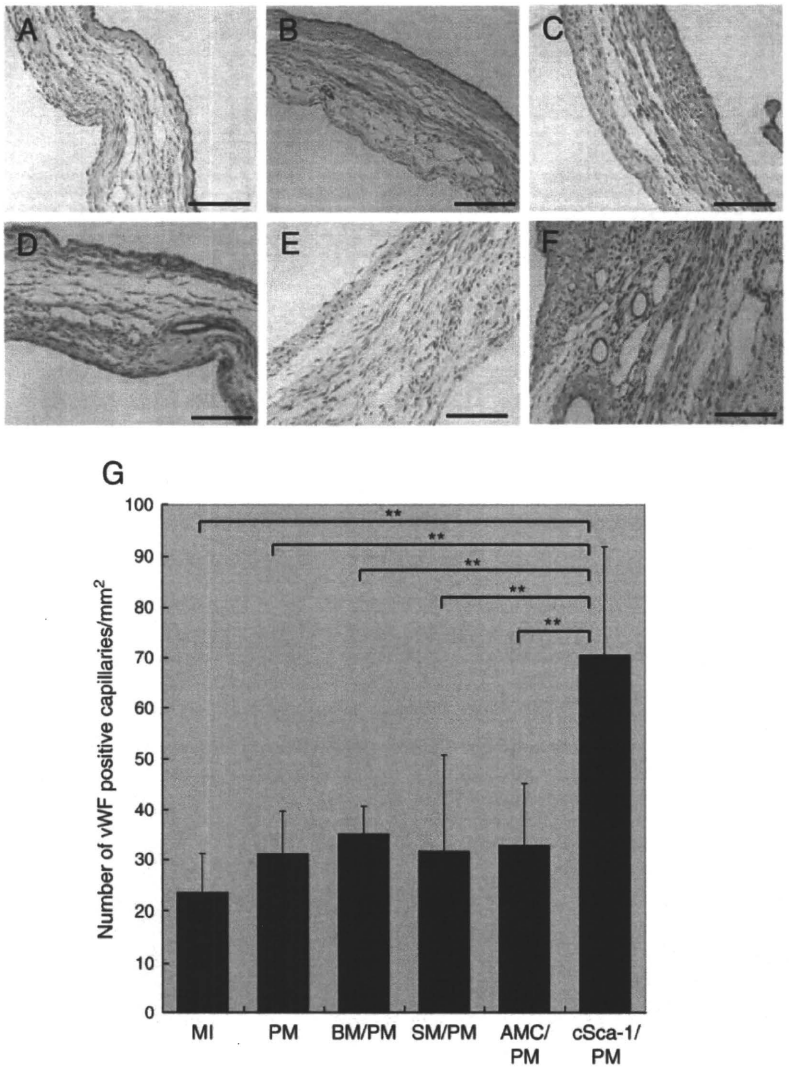

Fig. 2. Transplantation of cSca-1 with PM increases the number of vWF-positive capillary in infarct area. Representative images from the section of non-treated MI (A), PM-treated (B), BM/PM-treated (C), SM/PM-treated (D), AMC/PM-treated (E) and cSca-1/PM-treated (F) hearts stained for capillaries with anti-vWF antibodies. Bars are 100 μm. (G): Quantification of the number of vWF-positive capillaries 14 days after transplantation. Data are mean ± SD. **$p<0.01$ cSca-1/PM-treated vs. non-treated MI, PM-treated, BM/PM-treated, SM/PM-treated and AMC/PM-treated group.

(n = 4), 31.0 ± 8.6 in PM-treated (n = 8), 35.0 ± 5.6 in BM/PM-treated (n = 4), 31.6 ± 19.1 in SM/PM-treated (n = 4), 32.7 ± 12.5 in AMC/PM-treated (n = 7) and 70.4 ± 21.4 in cSca-1/PM-treated (n = 10) hearts (cSca-1/PM-treated hearts vs. non-treated MI, PM-treated, BM/PM-treated, SM/PM-treated and AMC/PM-treated hearts; $p<0.01$, Fig. 2G).

3.5. Transplantation of cSca-1 with PM increases the number of SMA-positive vessels in infarct area

At 2 weeks after transplantation, immunohistochemical staining for SMA indicated that more SMA-positive vessels exist in the infarct area of cSca-1/PM-treated heart (Fig. 3F) in comparison with non-treated MI (Fig. 3A), PM-treated (Fig. 3B), BM/PM-treated (Fig. 3C), SM/PM-treated (Fig. 3D) and AMC/PM-treated (Fig. 3E) hearts. The number of SMA-positive vessels per mm^2 was 17.6 ± 7.7 in non-treated MI (n = 5), 16.0 ± 8.8 in PM-treated (n = 7), 14.9 ± 3.5 in BM/PM-treated (n = 4), 20.0 ± 3.5 in SM/PM-treated (n = 4), 17.6 ± 9.3 in AMC/PM-treated (n = 4) and 36.3 ± 14.5 in cSca-1/PM-treated (n = 7) hearts (cSca-1/PM-treated hearts vs. non-treated MI, BM/PM-treated, SM/PM-treated and AMC/PM-treated hearts; $p<0.05$, cSca-1/PM-treated hearts vs. PM-treated hearts; $p<0.01$. Fig. 3G). These results suggested that enhancement of the formation of capillaries and conductive vessels at least partially account for the beneficial effect of transplantation of cSca-1/PM.

3.6. Transplantation of cSca-1 with PM reduces the frequency of apoptotic cardiomyocytes

Next we examined whether transplantation of cSca-1/PM complex inhibits apoptosis of cardiomyocytes. TUNEL staining of the heart 24 h after MI showed that many TUNEL- and SA actinin positive cardiomyocytes exist in the infarct and border areas of non-treated (Figs. 4A and D) and PM-treated (Figs. 4B and E) hearts. On the contrary the much lower number of apoptotic cardiomyocytes was observed in the infarct and border areas of cSca-1/PM-treated heart (Figs. 4C and F). In the normal area, there was no difference in the number of apoptotic cardiomyocytes among the three groups (Figs. 4G–I and 4J right panel). The percentage of TUNEL positive cardiomyocytes in the infarct area was 39.2 ± 5.8 in non-treated MI

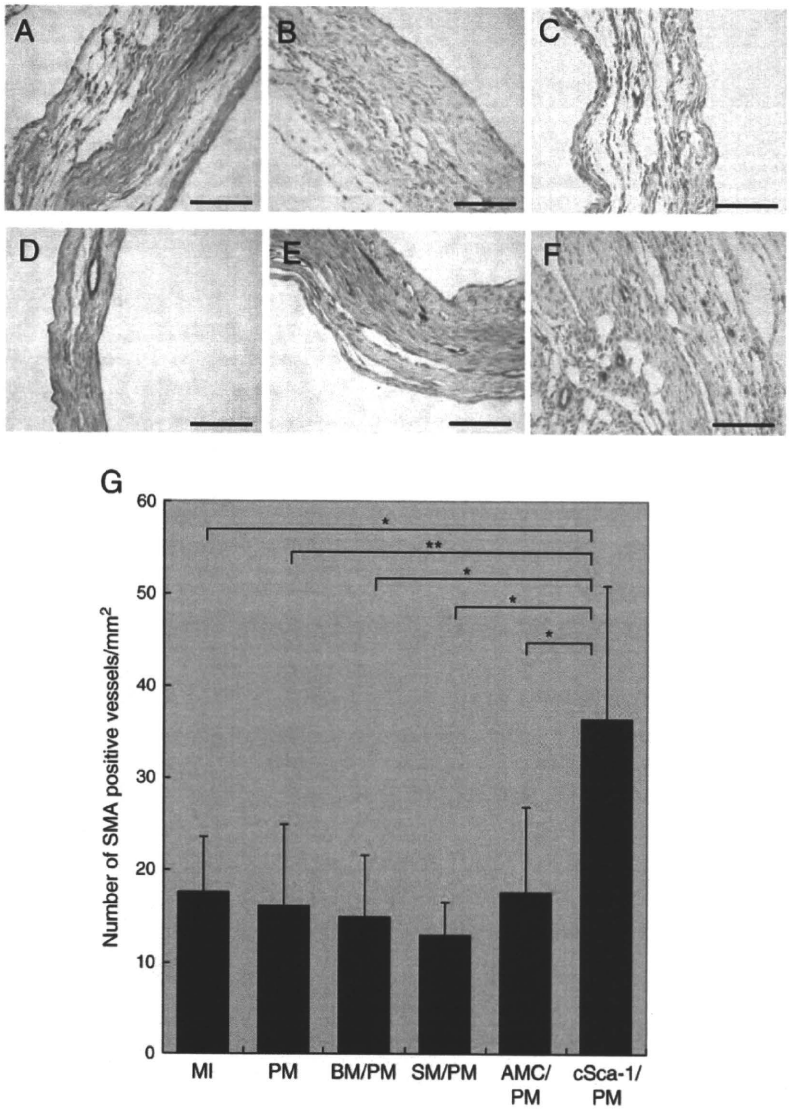

Fig. 3. Transplantation of cSca-1 with PM increases the number of SMA-positive vessels in an infarct area. Representative images from the section of non-treated MI (A), PM-treated (B), BM/PM-treated (C), SM/PM-treated (D), AMC/PM-treated (E) and cSca-1/PM-treated (F) hearts stained for vessels with anti-SMA antibodies. Bars are 100 μm. (G): Quantification of the number of SMA-positive vessels 14 days after transplantation. Data are mean ± SD. *p<0.05 cSca-1/PM-treated vs. non-treated MI, BM/PM-treated, SM/PM-treated and AMC/PM-treated group. **p<0.01 cSca-1/PM-treated vs. PM-treated group.

(n = 3), 54.0 ± 1.1 in PM-treated (n = 2), and 20.1 ± 6.3 in cSca-1/PM-treated (n = 4) hearts (cSca-1/PM-treated hearts vs. PM-treated hearts; p<0.01, cSca-1/PM-treated hearts vs. non-treated hearts; p<0.05. Fig. 4J left panel). The percentage of TUNEL positive cardiomyocytes in the border area was 33.8 ± 7.1 in non-treated MI (n = 3), 46.1 ± 9.6 in PM-treated (n = 2), 15.5 ± 10.0 in cSca-1/PM-treated (n = 4) hearts (cSca-1/PM-treated hearts vs. PM-treated hearts; p<0.05, Fig. 4J middle panel). There was no difference in the density of CD31-positive endothelial cells and the percentage of TUNEL positive endothelial cells in infarct, border and normal areas among the three groups (Supplemental Fig. 5).

3.7. Transplanted cells decrease during the first few days after transplantation due to non-apoptotic cell death

Next we examined the localization and frequency of engraftment of transplanted cells. At 1 day after transplantation, the percentage of GFP-positive cells per total cells in the infarct and border zone was 1.5% ± 0.84 in cSca-1/PM-treated, 2.5% ± 1.0 in AMC/PM-treated, 2.0% ± 1.1 in SM/PM-treated and 1.1% ± 0.70 in BM/PM-treated hearts (AMC/PM-treated vs. cSca-1/PM-treated and BM/PM-treated hearts; p<0.05, SM/PM-treated vs. BM/PM-treated hearts; p<0.05, Fig. 5A). The percentage of GFP-positive cells in the epicardial region was 10.8% ± 9.1 in cSca-1/PM-treated, 9.4% ± 6.8 in AMC/PM-treated, 11.3% ± 11.2 in SM/PM-treated and 15.3% ± 6.7 in BM/PM-treated hearts (Fig. 5A). There was no significant difference in the percentage of GFP-positive cells in the epicardial region among the cell types.

At 3 days after transplantation, the percentage of GFP-positive cells per total cells in the infarct and border zone was 0.97% ± 0.83 in cSca-1/PM-treated, 1.5% ± 1.2 in AMC/PM-treated, 1.0% ± 0.75 in SM/PM-treated and 0.84% ± 0.86 in BM/PM-treated hearts (Fig. 5B). The percentage of GFP-positive cells in the epicardial region was 4.4% ± 4.9 in cSca-1/PM-treated, 7.8% ± 6.3 in AMC/PM-treated, 6.2% ± 4.2 in SM/PM-treated and 7.6% ± 8.0 in BM/PM-treated hearts (Fig. 5B). There was no significant difference in the percentage of GFP-positive cells in both myocardium and epicardial region among the cell types. At 1 and

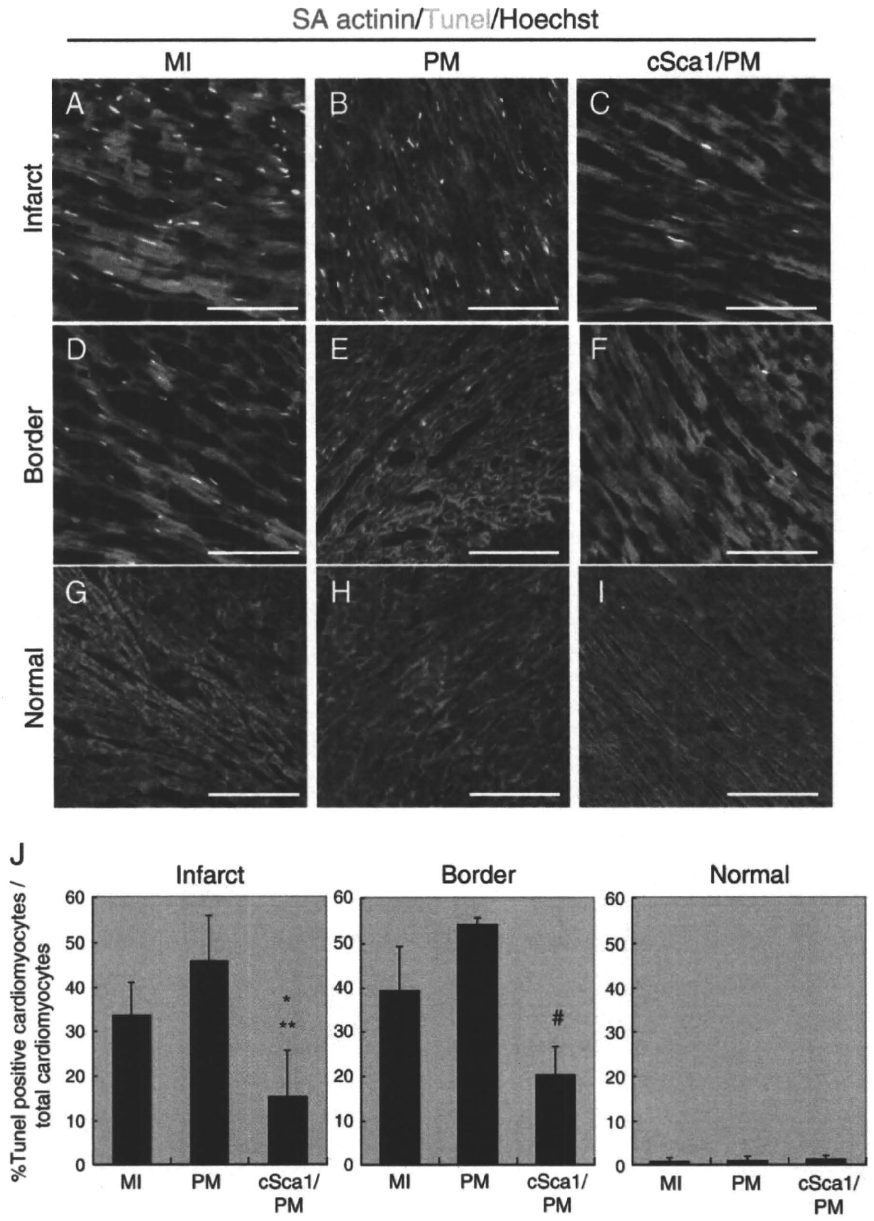

Fig. 4. Transplantation of cSca-1 with PM reduces the number of apoptotic cardiomyocytes. Representative images from the section of non-treated (A, D, G), PM-treated (B, E, H), and cSca-1/PM-treated (C, F, I) hearts stained by using the TUNEL method 24 h after MI. Upper, middle and bottom row represent infarct, border and normal areas, respectively. Red, sarcomeric alpha actinin; blue, nuclear staining (Hoechst 33258); green, TUNEL positive cardiomyocytes. Bars are 50 μm. (J): Quantification of the percentage of TUNEL positive cardiomyocytes in infarct, border and normal area 24 h after transplantation. Data are mean ± SD. #, $p<0.05$ cSca-1/PM-treated vs. PM-treated group. *$p<0.05$ cSca-1/PM-treated vs. non-treated MI group. **$p<0.01$ cSca-1/PM-treated vs. PM-treated group.

3 days after transplantation, a significantly higher percentage of GFP-positive cells was observed in the epicardial region in comparison with the myocardium in all of four cell types. Representative immunohistochemical images of GFP-expressing cells at 3 days after transplantation showed that scattered GFP-positive cells in the myocardium and epicardial surface (Supplement Figs. 4F to I, an image of non-labeled cSca-1/PM transplanted myocardium was presented as a negative control in E). Many of GFP-positive cells existed in the epicardial surface (white arrowheads in Supplement Figs. 4F to I).

To elucidate the cause of reduction of transplanted cells, we examined the frequency of apoptotic and non-apoptotic cell death in GFP-positive cells. Apoptosis was detected as TUNEL positive cells. Non-apoptotic cell death was defined on the basis of nuclear shrinkage [25]. At 1 day after transplantation, the percentage of nuclear shrunk non-apoptotic dead cells was 38.5% ± 30.8 in cSca-1/PM-treated, 58.3% ± 21.5 in AMC/PM-treated, 52.5% ± 27.2 in SM/PM-treated and 29.9% ± 35.0 in BM/PM-treated hearts (cSca-1/PM-treated and BM/PM-treated vs. AMC/PM-treated hearts; $p<0.05$, Fig. 5C). The percentage of apoptotic cells was 7.4% ± 17.7 in cSca-1/PM-treated, 7.3% ± 9.9 in AMC/PM-treated, 7.4% ± 14.0 in SM/PM-treated and 16.0% ± 22.6 in BM/PM-treated hearts (Fig. 5D). Representative immunohistochemical images of GFP-expressing cSca-1 transplanted heart revealed that GFP-positive nuclear shrunk non-apoptotic dead cSca-1 (white arrow heads in Fig. 5E), GFP and TUNEL

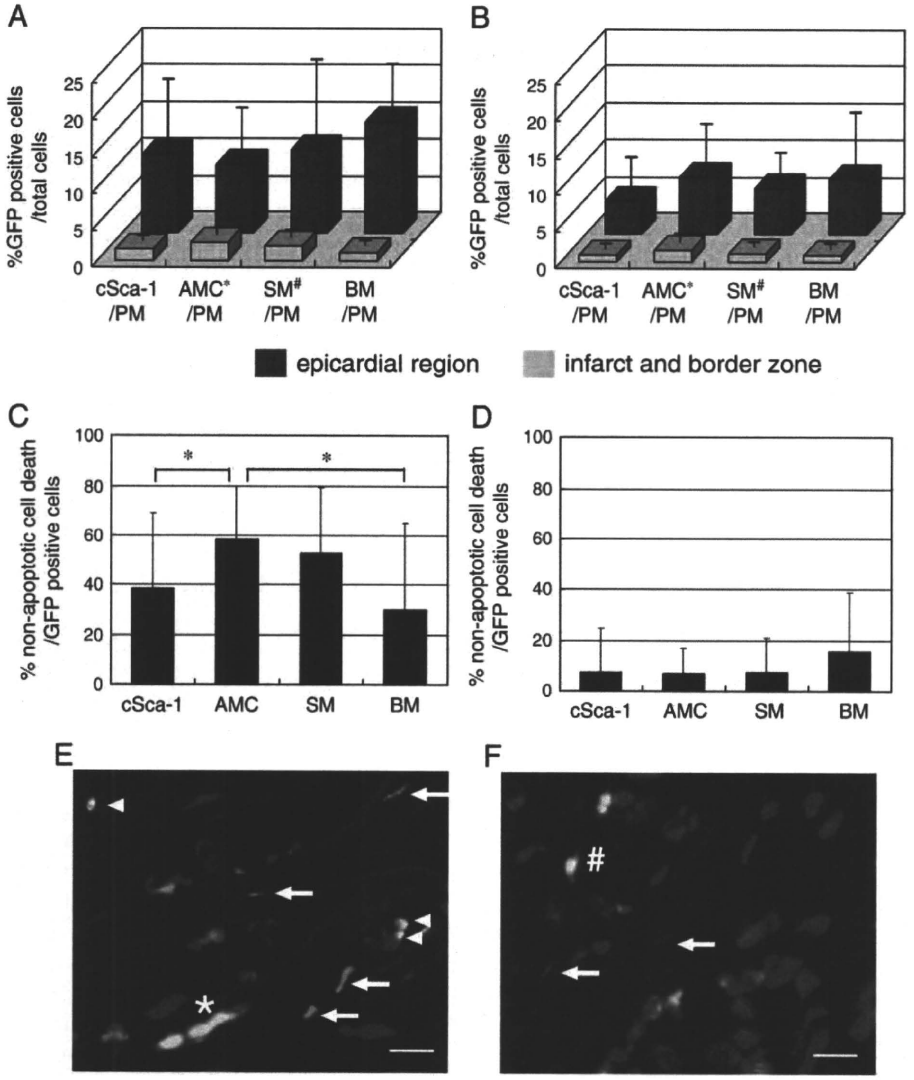

Fig. 5. Transplanted cells decrease within the first few days due to non-apoptotic cell death. Quantitative analysis of the percentage of GFP-positive cells per total cells at 1 day (A) and 3 days (B) after transplantation. The percentages of GFP-positive cells in the epicardium and in the myocardium were displayed separately. Data are obtained from 2 to 5 mice in each group and expressed as mean ± SD. *$p<0.05$ AMC/PM-treated vs. cSca-1/PM-treated and BM-treated group. #$p<0.05$ SM/PM-treated vs. BM/PM-treated group. Quantitative analysis of the percentage of non-apoptotic (C) and apoptotic cell death (D) in GFP-positive transplanted cells. Data are obtained from 3 mice in each group and expressed as mean ± SD. *$p<0.05$ cSca-1/PM-treated and BM/PM-treated group vs. AMC/PM-treated group. Immunohistochemical images of GFP-expressing cSca-1 transplanted heart (E and F). GFP-positive nuclear shrunk non-apoptotic dead cSca-1 (white arrow heads in E), GFP and TUNEL double-positive apoptotic cSca-1 (white sharp in F), TUNEL positive host apoptotic cells (white arrows in E and F) and viable GFP-positive transplanted cSca-1 (white asterisk in E) were indicated. Bars are 25 μm.

double-positive apoptotic cSca-1 (white sharp in Fig. 5F), TUNEL positive host apoptotic cells (white arrows in Fig. 5E and F) and viable GFP-positive transplanted cSca-1 (white asterisk in Fig. 5E).

These results suggest that non-apoptotic cell death may cause a significant reduction of transplanted cells during 1 to 3 days after transplantation. Although the frequency of transplanted AMC and SM was higher than that of cSca-1 and BM at 1 day after transplantation (Fig. 5A), vulnerability to non-apoptotic cell death was higher in AMC and SM in comparison with cSca-1 and BM, resulting in the identical degree of engraftment among the four types of transplanted cells at 3 days after transplantation.

3.8. cSca-1 transdifferentiate into smooth muscle cells and cardiomyocytes in vivo and secrete angiogenic factors

The percentage of GFP-positive cells at 7 days after transplantation was 0.21% ± 0.25 in cSca-1/PM-treated, 0.035% ± 0.090 in AMC/PM-treated, and 0.060% ± 0.096 in SM/PM-treated hearts (cSca-1/PM-treated vs. AMC/PM-treated hearts; $p<0.05$, Supplement Fig. 4J). GFP-positive cells were not detected in BM/PM-treated hearts. A group of GFP-positive cSca-1 cells, which co-express SA actinin was observed in infarct area (Figs. 6A and B). Co-expression of SA actinin was observed in approximately 66% of GFP-positive cSca-1 cells but not in GFP-positive AMC and SM. The frequency of GFP- and SMA-positive transplanted cSca-1 was ~1% of GFP-positive cells. Next we examined the cell fate of transplanted RFP-expressing cSca-1/PM by using confocal microscopy. Three days after transplantation, many elongated RFP-positive cSca-1 were observed beneath the epicardium (Fig. 6C) and in the middle of myocardium (Fig. 6D). Seven days after transplantation, some of RFP-positive cSca-1 were incorporated into the media of artery and express SMA (Fig. 6E). In addition some of the RFP-positive cSca-1 expressed SA actinin with a fine striated pattern (Fig. 6F). Immunofluorescent images of the non-labeled cSca-1/PM transplanted heart stained with anti-RFP antibodies in

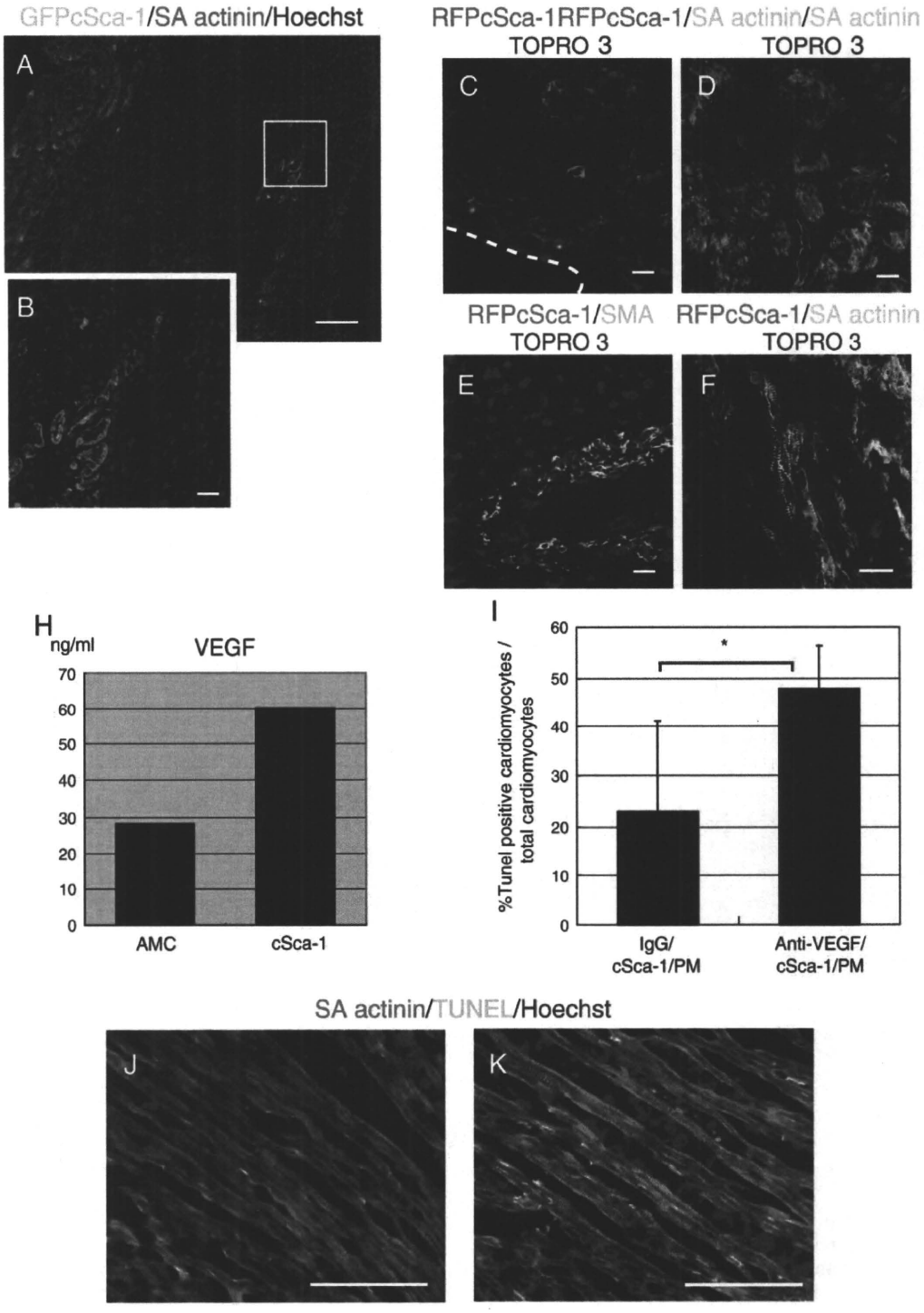

Fig. 6. cSca-1 transdifferentiate into smooth muscle cells and cardiomyocytes in vivo and secrete angiogenic factors. A low magnified immunofluorescent image of the heart at 7 days after transplantation of GFP-expressing cSca-1/PM (A). A group of cSca-1 (green) in the infract zone express SA actinin (red) (white square in A). A bar is 100 μm. A magnified image corresponding to the white square in A is presented as B. A bar is 20 μm. Nuclei are shown in blue. Immunofluorescence confocal images of engrafted RFP-expressing cSca-1 (red) (C–F). Engrafted cSca-1 cells existed under the epicardial surface (C, epicardium was indicated as a white dotted line) and in the middle of myocardium (D) at 3 days after transplantation. SA actinin and nuclei are shown in green and blue, respectively. Engrafted RFP-expressing cSca-1 (red) express SMA (E shown in green) and SA actinin (F shown in green) at 7 days after transplantation. Nuclei are shown in blue. Secretion of VEGF by cSca-1 and ADMC (H). Cell culture supernatants were analyzed by using Bio-Plex Suspension Array System. Values are means of duplicated samples. Quantitative analysis of the percentage of TUNEL positive cardiomyocytes per total cardiomyocytes in IgG/cSca-1/PM-treated and anti-VEGF/cSca-1/PM-treated heart at 1 day after transplantation (I). Data are obtained from 2 mice in each group and expressed as mean ± SD. *$p<0.05$ IgG/cSca-1/PM-treated vs. anti-VEGF/cSca-1/PM-treated group. Immunohistochemical images of TUNEL positive cardiomyocytes in IgG/cSca-1/PM-treated (J) and anti-VEGF/cSca-1/PM-treated (K) heart. The mice were subjected to immunohistochemical analysis at 1 day after transplantation. TUNEL staining was in green, SA actinin was in red and nuclei were in blue. Bars are 100 μm.

combination with anti-SA actinin or anti-SMA were presented as negative control (Supplemental Figs. 4K and L). A highly magnified confocal z-stack image showed a sarcomere-positive cardiomyocyte derived from RFP-expressing cSca-1 (Supplemnatal movie 1). A red fluorescent signal co-localized with a green signal from SA actinin throughout the stacked images, suggesting that two markers are stained in the same cells. The cells presented in Supplemnatal Movie 1 posses a single nucleus but not double nuclei, suggesting that cell fusion, which is characterized by heterokaryon formation is not likely. These results suggest that transplanted cSca-1 engraft better than AMC, SM and BM, maintain the character of cardiac progenitors and differentiate into multiple types of cells including smooth muscle cells and cardiomyocytes. As shown in Figs. 2 and 3, cSca-1 enhanced angiogenesis when transplanted. Thus next we examined the concentration of angiogenic growth factors such as basic FGF, PDGF-bb and VEGF in the culture medium of AMC and cSca-1. Both cells secrete lots of VEGF and little of basic FGF and PDGF-bb is in the culture medium, and the concentration of VEGF in the culture medium of cSca-1 was approximately two times higher than that of AMC, suggesting that VEGF mediates cSca-1-induced angiogenesis as a paracrine factor (Fig. 6H, Supplemental Figs. 6A and B). To examine whether VEGF is a prerequisite for preventing apoptosis of cardiomyocytes, we neutralized VEGF in cSca-1/PM with anti-VEGF antibody just before transplantation. At 1 day after transplantation, the percentage of TUNEL positive cardiomyocytes in border and infarct area was $23.0\% \pm 15$ in control IgG/cSca-1/PM-treated and $47.8\% \pm 8.6$ in anti-VEGF/cSca-1/PM-treated hearts (IgG/cSca-1/PM-treated hearts vs. anti-VEGF/cSca-1/PM-treated; $p \leq 0.05$, Fig. 6I). Immunofluorescent images of TUNEL staining revealed that more TUNEL positive cardiomyocytes exist in IgG/cSca-1/PM-treated (Fig. 6J) than in anti-VEGF/cSca-1/PM-treated hearts (Fig. 6K).

4. Discussion

Somatic cells from various organs such as skeletal muscle, bone marrow and adipose tissue are considered to be safe and become good candidates for cells transplanted into the injured heart. However, currently we do not have enough information to answer fundamental questions, what are the optimal cells and how cell transplantation shows beneficial effects. Here we first reported that cardiac progenitor cells are the most effective for cardiac repair in comparison with skeletal, bone marrow, or adipose tissue-derived cells. Cardiac progenitor cells reduced apoptosis of cardiomyocytes and promoted angiogenesis leading to reduce the infarct area and restore cardiac function through both transdifferentiation and paracrine effects. Furthermore we have shown that a self-assembling nanopeptide, PM is a useful biological scaffold, which can deliver and hold the cells in the myocardium and epicardial space.

Many 3-dimensional materials have been investigated for myocardial scaffold, including fibrin glue, poly lactic-coglycolic acid (PLGA), gelatin hydrogels, and hyaluronic acid (HA) hydrogels [7]. Once the cells adapt to 3-dimensional milieus, the cells migrate, proliferate and function according to the multi-directional molecular and mechanical signals like an organized tissue. However, there are substantial challenges for existing materials, including stimulation of the host inflammatory response, excessively large pore size and fiber diameter and toxic degradation [26]. Self-assembling nanopeptides such as PM are an artificial material without animal-derived proteins. Hydrogels formed by self-assembling peptides have very small pore sizes that promote endothelial adhesion and capillary formation, but still allow rapid migration of cells [22]. When injected into the myocardium, nanofibers rapidly polymerize at physiological pH and osmolality, resulting in the entrapment of the transplanted cells and preventing from leakage. In addition the rigidity of hydrogel can be tuned by the concentration of a nanopeptide solution, enabling us to deliver both the forms of injectable and slab hydrogel. These properties of nanopeptides may enhance the engraftment of a larger number of cells in comparison with a simple direct injection, leading to reduced infarct size as shown in Supplemental Figs. 1G–J.

Davis et al. have reported that injected cell free nanopeptides recruit endothelial cells followed by immature cardiomyocyte over 4 weeks [12], however, our data showed that transplantation of cSca-1/PM but not PM itself attenuates infarct area and cardiac remodeling at 2 weeks after MI. These findings suggest that the effect of assembled nanofiber-mediated tissue repair on cardiac function is limited and that the existence of cells in the nanofiber scaffold is important for cardiac repair. Among the variable cell types we tested, cSca-1 appeared to be the best cell source for transplantation. cSca-1 were derived from primary Sca-1 positive cardiac progenitor cells, which differentiate into mature cardiomyocytes [17]. Although transplanted cSca-1 differentiated into cardiomyocytes and vascular smooth muscle cells in the infarct area (Figs. 6A–F), a contribution of *de novo* cSca-1-derived cardiomyocytes on cardiac regeneration may not be a major factor because RFP-positive cSca-1-derived cells covered a very small area in the infarct area (Fig. 6A).

It has been reported that paracrine factors from transplanted cells are one of the major factors, which mediate myocardial survival and repair [27,28]. Analysis of secreted angiogenic growth factors suggests that VEGF is one of the factors through which cSca-1 mediate angiogenesis and cardiomyocyte survival (Fig. 6H–K, Supplemental Fig. 6A and B). Cardiac endothelial–myocardial signaling is a prerequisite for normal cardiac development and growth [29]. VEGF is mainly secreted from cardiomyocytes and plays an important role in both angiogenesis and vasculogenesis through promotion of endothelial survival, proliferation, migration and differentiation [30]. VEGF is one of the factors increasing the number of mobilized and circulating endothelial progenitor cells [31,32]. Flk-1, CD144 and CD31 have been reported to be markers of mobilized and peripheral circulating EPC in the various stages of maturity [33,34]. When the number of recruited Flk-1-, CD144- and CD31-positive cells was examined, no significant difference was observed among cSca-1/PM, AMC/PM, SM/PM and BM/PM, suggesting that cSca-1-mediated recruitment of endothelial progenitor cells may not be a major mechanism of angiogenesis in this model (Supplemental Fig. 7).

Recently it has been reported that VEGF prevents deterioration of cardiac function after pathological hypertrophy and MI through coordinated angiogenesis [35,36]. Since many endothelial cells were directed to apoptosis immediately after MI, supplemental VEGF from cSca-1 may enhance angiogenesis over 2 weeks and contribute to restoration of cardiac function. During angiogenesis, PDGF-bb plays an important role in proliferation and migration of mural cells, resulting in vessel maturation [37]. The amount of PDGF-bb in cSca-1/PM injected myocardium was more than that in MI and AMC/PM injected tissue at 3 days after transplantation (Supplemental Fig. 6C), suggesting that VEGF derived from cSca-1 may support endothelial cells to secrete PDGF-bb, resulting in the formation of SMA-positive mature vessels. In contrast to endothelial cells, transplantation of cSca-1/PM rescued cardiomyocyte apoptosis at 24 h after MI. Our results suggest that VEGF is one of the factor, which protect cardiomyocytes from apoptosis. PM has a nature to bind to various proteins such as cytokines and immuno-globulins and release them slowly [38]. Therefore it is likely that injected anti-VEGF antibodies bind to PM, stay with neighboring cSca-1, and neutralize secreted VEGF from cSca-1 rather than intrinsic VEGF, resulting in the abrogation of VEGF-mediated protection of cardiomyocytes. Dai et al. have reported that cardiomyocyte-derived intrinsic VEGF is not enough to protect cardiomyocytes against oxidative stress but the addition of exogenous VEGF protects cardiomyocytes effectively [39]. Their findings are concordant with our results in terms of the importance of additive VEGF. Recently we have reported that cSca-1 but not AMC secrete a large amount of soluble VCAM-1, which attenuate cardiac remodeling after MI through promoting angiogenesis and survival of

cardiomyocytes [18]. Therefore soluble VCAM-1 as well as VEGF or other unidentified cardiac progenitor cell-derived factors may be organized to mediate cardiac anti-apoptotic effect of transplanted cSca-1/PM.

We have shown that PM can be a useful biomaterial, which assures a safe and effective delivery of the cells into the myocardium. Recently Gelain et al. have reported the evidence for slow and sustained cytokine release from PM scaffolds [38]. During 1 to 3 days after transplantation, 1.0–1.5% and 4–10% of cSca-1 were observed in the myocardium and epicardial layer, respectively. Therefore PM may play a critical role in holding cSca-1 and support sustained release of VEGF, sVCAM-1 or other cSca-1 specific molecules. However, when cSca-1/PM was transplanted into the mice at 7 days after myocardial infarction, the infarct size was identical between cSca-1/PM-treated and PM-treated mice at 2 weeks after transplantation (supplemental Fig. 6D–F). Therefore PM is not enough to support a long-term proliferation, engraftment or differentiation of transplanted cells in the established infarct heart tissue. Self-assembling nanopeptide can be modified in a variety of manners, allowing cell-specific signals to be delivered. For example nanofiber scaffold containing RGD binding sequence significantly promoted proliferation of mouse pre-osteoblast [40]. Moreover, alkaline phosphatase (ALP) activity and osteocalcin secretion, which are early and late markers for osteoblastic differentiation, were also significantly increased [40]. Silva et al. synthesized self-assembling peptides containing an IKVAV laminin motif, in which the neuronal precursors differentiated into neurons with extensive processes, while very few cells differentiated into astrocytes [41]. These tailor-made peptides have the ability to modulate bidirectional signals between nanopeptides and transplanted cells, enabling us to create a forever 3-dimensional cardiac graft, which substitutes the scar tissue after myocardial infarction, leading to prevention of cardiac remodeling and improvement of cardiac function.

Supplementary materials related to this article can be found online at doi:10.1016/j.yjmcc.2010.09.015.

Acknowledgments

The authors thank A. Furuyama for the excellent technical assistance. This work was supported by a Grant-in-Aid for Scientific Research, Developmental Scientific Research, and Scientific Research on Priority Areas from the Ministry of Education; Science, Sports, and Culture, Mitsubishi Pharma Research Foundation, and Health and Labour Sciences Research Grants; and Takeda Science Foundation. We thank 3-D Matrix, Ltd. for providing Puramatrix™.

References

[1] Passier R, van Laake LW, Mummery CL. Stem-cell-based therapy and lessons from the heart. Nature 2008;453:322–9.
[2] Dimmeler S, Burchfield J, Zeiher AM. Cell-based therapy of myocardial infarction. Arterioscler Thromb Vasc Biol 2008;28:208–16.
[3] Menasché P, Alfieri O, Janssens S, McKenna W, Reichenspurner H, Trinquart L, et al. The Myoblast Autologous Grafting in Ischemic Cardiomyopathy (MAGIC) trial: first randomized placebo-controlled study of myoblast transplantation. Circulation 2008;117:1189–200.
[4] Rosenzweig A. Cardiac cell therapy-mixed results from mixed cells. N Engl J Med 2006;355:1274–7.
[5] Dow J, Simkhovich BZ, Kedes L, Kloner RA. Washout of transplanted cells from the heart: a potential new hurdle for cell transplantation therapy. Cardiovasc Res 2005;67:301–7.
[6] Zhang M, Methot D, Poppa V, Fujio Y, Walsh K, Murry CE, et al. Cardiomyocyte grafting for cardiac repair: graft cell death and anti-death strategies. J Mol Cell Cardiol 2001;33:907–21.
[7] Eschenhagen T, Zimmermann WH. Engineering Myocardial Tissue Circ Res 2005;97:1220–31.
[8] Zhang S, Holmes T, Lockshin C, Rich A. Spontaneous assembly of a self-complementary oligopeptide to form a stable macroscopic membrane. Proc Natl Acad Sci USA 1993;90:3334–8.
[9] Thornhoff JR Lou, DI Jordan PM, Zhao X, Wu P. Compatibility of human fetal neural stem cells with hydrogel biomaterials in vitro. Brain Res 2008;1187:42–51.
[10] Hamada K, Hirose M, Yamashita T, Ohgushi H. Spatial distribution of mineralized bone matrix produced by marrow mesenchymal stem cells in self-assembling peptide hydrogel scaffold. J Biomed Mater Res 2008;84:128–36.
[11] Narmoneva DA, Oni O, Sieminski AL, Zhang S, Gertler JP, Kamm RD, et al. Self-assembling short oligopeptides and the promotion of angiogenesis. Biomaterials 2005;26:4837–46.
[12] Davis ME, Motion JP, Narmoneva DA, Takahashi T, Hakuno D, Kamm RD, et al. Injectable self-assembling peptide nanofibers create intramyocardial microenvironments for endothelial cells. Circulation 2005;111:442–50.
[13] Ellis-Behnke RG, Liang YX, You SW, Tay DK, Zhang S, So KF, et al. Nano neuro knitting: peptide nanofiber scaffold for brain repair and axon regeneration with functional return of vision. Proc Natl Acad Sci USA 2006;103:5054–9.
[14] Hsieh PCH, Davis ME, Gannon J, MacGillivray C, Lee RT. Controlled delivery of PDGF-BB for myocardial protection using injectable self-assembling peptide nanofibers. J Clin Invest 2006;116:237–48.
[15] Davis ME, Hsieh PC, Takahashi T, Song Q, Zhang S, Kamm RD, et al. Local myocardial insulin-like growth factor 1 (IGF-1) delivery with biotinylated peptide nanofibers improves cell therapy for myocardial infarction. Proc Natl Acad Sci USA 2006;103:8155–60.
[16] Okabe M, Ikawa M, Kominami K. 'Green mice' as a source of ubiquitous green cells. FEBS Lett 1997;407:313–9.
[17] Matsuura K, Nagai T, Nishigaki N, Oyama T, Nishi J, Wada H, et al. Adult cardiac Sca-1-positive cells differentiate into beating cardiomyocytes. J Biol Chem 2004;279:11384–91.
[18] Matsuura K, Honda A, Nagai T, Fukushima N, Iwanaga K, Tokunaga M, et al. Transplantation of cardiac progenitor cells ameliorates cardiac dysfunction after myocardial infarction in mice. J Clin Invest 2009;119:2204–17.
[19] Planat-Bénard V, Menard C, Andre M, Puceat M, Perez A, Garcia-Verdugo JM, et al. Spontaneous cardiomyocyte differentiation from adipose tissue stroma cells. Circ Res 2004;94:223–9.
[20] Rando TA, Blau HM. Primary mouse myoblast purification, characterization, and transplantation for cell-mediated gene therapy. J Cell Biol 1994;125:1275–87.
[21] Matsuura K, Wada H, Nagai T, Iijima Y, Minamino T, Sano M, et al. Cardiomyocytes fuse with surrounding noncardiomyocytes and reenter the cell cycle. J Cell Biol 2004;167:351–63.
[22] Yokoi H, Kinoshita T, Zhang S. Dynamic reassembly of peptide RADA16 nanofiber scaffold. Proc Natl Acad Sci USA 2005;102:8414–9.
[23] Gao XM, Dart AM, Dewar E, Jennings G, Du XJ, et al. Serial echocardiographic assessment of left ventricular dimensions and function after myocardial infarction in mice. Cardiovasc Res 2000;45:330–8.
[24] Schäffler A, Büchler C. Adipose tissue-derived stromal cells—basic and clinical implications for novel cell-based therapies. Stem Cells 2007;25:818–27.
[25] Shinzawa K, Tsujimoto Y. PLA2 activity is required for nuclear shrinkage in caspase-independent cell death. J Cell Biol 2003;163:1219–30.
[26] Davis ME, Hsieh PC, Grodzinsky AJ, Lee RT. Custom design of the cardiac microenvironment with biomaterials. Circ Res 2005;97:8–15.
[27] Hinkel R, El-Aouni C, Olson T, Horstkotte J, Mayer S, Müller S, et al. Thymosin β4 is an essential paracrine factor of embryonic endothelial progenitor cell mediated cardioprotection. Circulation 2008;117:2232–40.
[28] Mirotsou M, Zhang Z, Deb A, Zhang L, Gnecchi M, Noiseux N, et al. Secreted frizzled related protein 2 (Sfrp2) is the key Akt-mesenchymal stem cell-released paracrine factor mediating myocardial survival and repair. Proc Natl Acad Sci USA 2007;104:1643–8.
[29] Brutsaert DL. Cardiac endothelial–myocardial signaling: its role in cardiac growth, contractile performance, and rhythmicity. Physiol Rev 2003;83:59–115.
[30] Ferrara N. Molecular and biological properties of vascular endothelial growth factor. J Mol Med 1999;77:527–43.
[31] Asahara T, Murohara T, Sullivan A, Silver M, van der Zee R, Li T, et al. Isolation of putative progenitor endothelial cells for angiogenesis. Science 1997;275:964–7.
[32] Kalka C, Masuda H, Takahashi T, Gordon R, Tepper O, Gravereaux E, et al. Vascular endothelial growth factor$_{165}$ gene transfer augments circulating endothelial progenitor cells in human subjects. Circ Res 2000;86:1198–202.
[33] Hristov M, Erl W, Weber PC. Endothelial progenitor cell: mobilization, differentiation, and homing. Arterioscler Thromb Vasc Biol 2003;23:1185–9.
[34] Wu BJ, Midwinter RG, Cassano C, Beck K, Wang Y, Changsiri D, et al. Heme oxygenase-1 increases endothelial progenitor cells. Arterioscler Thromb Vasc Biol 2009;29:1537–42.
[35] Shiojima I, Sato K, Izumiya Y, Schiekofer S, Ito M, Liao R, et al. Disruption of coordinated cardiac hypertrophy and angiogenesis contributes to the transition to heart failure. J Clin Invest 2005;115:2108–18.
[36] Tirziu D, Chorianopoulos E, Moodie KL, Palac RT, Zhuang ZW, Tjwa M, et al. Myocardial hypertrophy in the absence of external stimuli is induced by angiogenesis in mice. J Clin Invest 2007;117:3188–97.
[37] Hoch RV, Soriano P. Roles of PDGF signaling in animal development. Development 2003;130:4769–84.
[38] Gelain F, Unsworth LD, Zhang S. Slow and sustained release of active cytokines from self-assembling peptide scaffolds. J Control Release 2010;42:231–9.
[39] Dai Y, Xu M, Wang Y, Pasha Z, Li T, Ashraf M. HIF-1alpha induced-VEGF overexpression in bone marrow stem cells protects cardiomyocytes against ischemia. J Mol Cell Cardiol 2007;42:1036–44.
[40] Horii A, Wang X, Gelain F, et al. Biological designer self-assembling peptide nanofiber scaffolds significantly enhance osteoblast proliferation, differentiation and 3-D migration. PLoS ONE 2007;2:e190.
[41] Silva GA, Czeisler C, Niece KL, et al. Selective differentiation of neural progenitor cells by high-epitope density nanofibers. Science 2004;303:1352–5.

Glossary

AAR: area at risk
AMC: adipose tissue-derived mesenchymal cells
AMC/PM: adipose tissue-derived mesenchymal cells with Puramatrix™
BM: bone marrow mononuclear cells
BM/PM: bone marrow mononuclear cells with Puramatrix™
BP: blood pressure
BW: body weight
cSca-1: clonal stem cell antigen-1 positive cells
cSca-1/PM: clonal stem cell antigen-1 positive cells with Puramatrix™
FGF: fibroblast growth factor
HR: heart rate
HW: heart weight
LVIDD: left ventricular internal diastolic diameter
INF: infarct size
LVISD: left ventricular internal systolic diameter
MI: myocardial infarction
PDGF: platelet-derived growth factor
PM: Puramatrix™
RFP: red fluorescent protein
SA actinin: sarcomeric alpha actinin
SM: skeletal myoblasts
SMA: alpha-smooth muscle cell actin
SM/PM: skeletal myoblasts with Puramatrix™
VEGF: vascular endothelial growth factor
vWF: von Willebrand factor

Hypertension Research (2010) 33, 1289–1297

www.nature.com/hr

ORIGINAL ARTICLE

Comparison of angiotensin II type 1-receptor blockers to regress pressure overload-induced cardiac hypertrophy in mice

Lei Li[1,2,4], Ning Zhou[1,4], Hui Gong[2], Jian Wu[1,2], Li Lin[1], Issei Komuro[3], Junbo Ge[1,2] and Yunzeng Zou[1,2]

Angiotensin II (AngII) type 1-receptor blockers (ARBs) have been effectively used not only in the treatment of hypertension but also in cardiac protection. However, whether and why there are differences in these effects still remain unclear. Here we compared the effects of five commonly used ARBs (Candesartan, Olmesartan, Losartan, Telmisartan and Valsartan) on pressure overload-induced cardiac hypertrophy in mice model. Pressure overload was produced by constriction of the transverse aorta (TAC) for 2 weeks, which induced a significant elevation of blood pressure; ARBs or saline was administered through a stomach tube; Cardiac hypertrophy was evaluated by transthoracic echocardiography, cardiac histology and specific gene expression analyses. Although all the five ARBs, which did not repress the elevation of left ventricular pressure after TAC, attenuated the development of cardiac hypertrophy in the wild-type mice, the degrees of regression by Candesartan, Olmesartan and Losartan tended to be larger than those by Telmisartan and Valsartan. Furthermore, in *angiotensinogen*-knockout mice lacking endogenous AngII, TAC-induced cardiac hypertrophy was regressed by Candesartan, Olmesartan and Losartan but not by Telmisartan and Valsartan administration. Our data suggest that Candesartan, Olmesartan and Losartan can effectively inhibit pressure overload-induced cardiac hypertrophy even in the absence of AngII, whereas Telmisartan and Valsartan could exert the inhibitory effects only in the presence of AngII.
Hypertension Research (2010) **33**, 1289–1297; doi:10.1038/hr.2010.182; published online 14 October 2010

Keywords: Angiotensin II; Angiotensin II type 1-receptor blockers; cardiac hypertrophy; pressure overload

INTRODUCTION

Cardiac hypertrophy is not only a physiologically adaptive state before heart failure, but also an independent risk factor of major cardiac events.[1] Although there are many factors that can induce cardiac hypertrophy, hypertensive stimulation is a major hypertrophy-inducing factor.[2,3] Angiotensin II (AngII) and its type 1-receptor (AT1-R) have been known to be greatly involved in pressure overload-induced cardiac hypertrophy.[4,5] AT1-R blockers (ARBs) are clinically available as a highly effective and well-tolerated class of drugs for the treatment of hypertension. In addition, a variety of clinical evidences have shown that ARBs provide cardiovascular protection beyond blood pressure (BP) lowering.[6] Especially, ARB administration effectively prevents cardiac hypertrophy and improves the cardiovascular outcomes in patients with hypertension.[6,7] At present, there are several ARBs widely used in clinics, such as Losartan, Irbesartan, Telmisartan, Candesartan, Valsartan, Olmesartan and so on. Although some of them have been shown to have more beneficial effects than other types of antihypertensive agents such as β-adrenergic receptor blockers and calcium channel blockers, there are also reports indicating that cardiovascular outcomes by ARB-based treatment do not differ from those by other agent-based treatment.[8,9] We therefore supposed whether there were differences in cardiac protection among ARBs besides antihypertensive potency.

AT1-R is a member of the G protein-coupled receptor superfamily[10] and ARBs are highly selective in binding to the AT1-R and blocking diverse effects mediated by AT1-R.[6,11,12] Structurally, ARBs not only have the common biphenyl-tetrazole ring but also the unique side chains, which contribute to drug-specific differences in pharmacokinetic and pharmacodynamic properties and antihypertensive potency.[6,13] Many *in vitro* studies including ours have suggested that the effects of ARBs on suppression of AT1-R activation differ.[11,12,14] However, a rigorous *in vivo* comparison of different ARBs to regress pressure overload-induced cardiac hypertrophy has not been performed. Moreover, we have recently reported that Candesartan inhibited activation of AT1-R and attenuated cardiac hypertrophy induced

[1]Central Laboratory, Shanghai Institute of Cardiovascular Diseases, Zhongshan Hospital, Fudan University, Shanghai, China; [2]Research Center for Cardiovascular Diseases, Institutes of Biomedical Sciences, Fudan University, Shanghai, China and [3]Department of Cardiovascular Science and Medicine, Chiba University Graduate School of Medicine, Chiba, Japan
[4]These authors contributed equally to this work.
Correspondence: Professor J Ge or Professor Y Zou, Institutes of Biomedical Sciences, Shanghai Institute of Cardiovascular Diseases, Zhongshan Hospital, Fudan University, 180 Feng Lin Road, Shanghai 200032, China.
E-mail: jbge@zs-hospital.sh.cn or zou.yunzeng@zs-hospital.sh.cn
Received 6 May 2010; revised 9 July 2010; accepted 13 July 2010; published online 14 October 2010